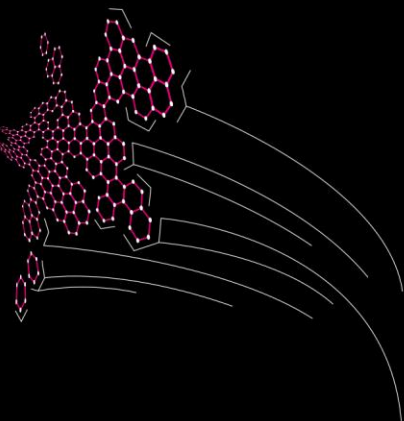
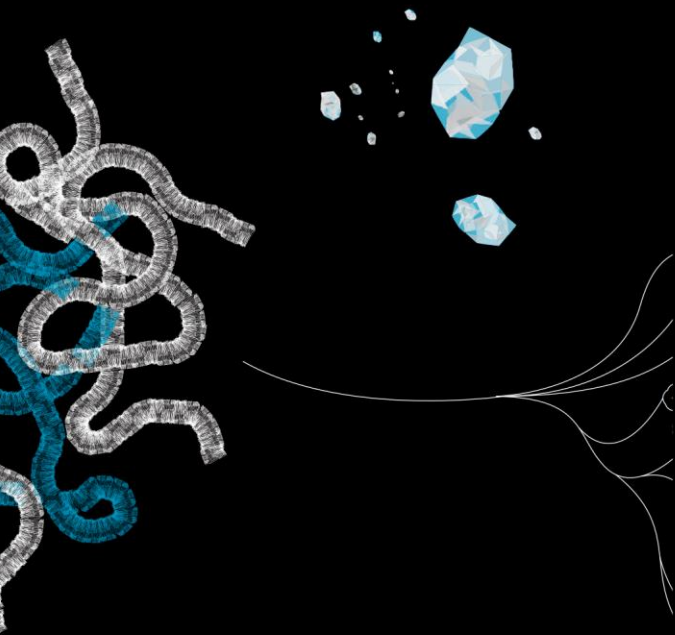


TURBULENCE

IN SCOUR HOLES OF SHARP BENDS



MSc Thesis
Civil Engineering and Management

Rik Posthumus

UNIVERSITY OF TWENTE.

TURBULENCE

IN SCOUR HOLES OF SHARP BENDS

Study about hydrodynamic processes in a scour hole of a sharp bend in the Mahakam River, Indonesia

MSc Thesis

CIVIL ENGINEERING AND MANAGEMENT
River and Coastal Engineering

Author

Rik Posthumus

Graduation committee

Dr. B. Vermeulen

Dr. K. M. Wijnberg

University of Twente - September 2017

“Ik weet niet zo veel. Ik weet niet wat goed en wat slecht is. Ik heb vermoedens, niet de waarheid. Maar ik geloof wel dat die er is. Hierboven. Daarachter. Dat je die aan kunt raken. Ik geloof dat er een *zijn* van de dingen is - dat *de* werkelijkheid bestaat en daarom ook de waarheid van de wereld.

Daar zijn de mensen naar op zoek. Er worden liederen over haar gezongen, en in de kranten schrijven journalisten elke dag aan haar voort, en natuurkundigen rekenen haar tegemoet, en soms wordt ze aangeraakt en soms in een paar dichtregels samengeperst, en soms is zij totaal afwezig, en soms komt ze mee in iets wat gemaakt wordt. Misschien in een stuk van Brahms, en weer weet je niet waar je moet zijn om het vast te pakken. Tussen de regels? Tussen de sleutel en de eerste maat? Moet je aan de vlaggetjes van de achtste noten trekken, of moet je juist je vuist in de schallende hoorns steken of de woorden uit je hoofd leren en elke dag weer opzeggen?”

Mintijteer – Esther Maria Magnis

PREFACE

Enschede, september 2017

Als een 'natuurkundige de waarheid tegemoet rekenen'. Een prachtige omschrijving van het fascinerende proces waar ik de afgelopen maanden mee bezig ben geweest. Daarin werd ik echter ook telkens geconfronteerd met het feit dat ik slechts in staat ben tot vermoedens te komen, de waarheid laat zich niet vangen in een paar berekeningen. Toch hoop ik dat mijn pogingen om deze verborgen waarheden uit de natuur te beschrijven, mogen helpen om ze iets beter te begrijpen. Om ze te benaderen en aan te raken, en in verwondering de uitkomsten te kunnen aanschouwen.

Tijdens mijn afstuderen ben ik door vele mensen op verschillende manieren geholpen, en hen wil ik graag bedanken. Als eerste Bart, die mijn dagelijks begeleider was. Regelmatig waren mijn inspanningen om MatLab te laten doen wat ik wilde tot mislukken gedoemd. Ik kon dan altijd bij Bart terecht, die de fout vaak snel gevonden had. Ook kreeg ik de nodige nuttige tips en feedback, waarmee ik stappen kon zetten die ik zelf lastig vond om te maken. Nuttige feedback kreeg ik ook van Kathelijne. Het is altijd fijn als iemand die wat verder van het onderwerp af staat er een blik op werpt. Er komen dan andere dingen aan het licht, die net zo belangrijk zijn als feedback op de ingewikkelde inhoud. Bart en Kathelijne: bedankt!

Daarnaast wil ik mijn familie, vrienden en studiegenoten bedanken. In onze afstudeerkamer hebben we de afgelopen maanden hard gewerkt, maar was er ook altijd genoeg tijd voor gezelligheid. Bovendien hielp de aanwezigheid van de anderen om niet de kantjes ervan af te lopen. Als eerste naar huis gaan in de loop van de middag, voelde toch altijd een beetje ongemakkelijk. Buiten het leven op de universiteit heb ik ook tijdens mijn afstuderen nog genoeg leuke dingen met familie en vrienden kunnen doen. Hoewel ik het niet met zekerheid kan zeggen, vermoed ik dat die afleiding een belangrijke bijdrage heeft geleverd aan dit rapport.

Tot slot wil ik vanaf deze plaats een diepe buiging maken voor mijn moeder. Ik kan alleen maar grote bewondering hebben voor de manier waarop zij het leven heeft opgepakt, nadat mijn vader 17 jaar geleden zijn strijd tegen de kanker verloor. In die jaren heeft zij er alles aan gedaan om het leven voor mij en mijn broertjes zo normaal mogelijk te laten zijn. En niet omdat anderen dat van haar verwachtten, maar enkel omdat ze zo enorm veel van ons houdt. Zulke liefde overstijgt het niveau van vermoedens en hoort bij de grootste waarheden van het leven. Mem, bedankt!

Rik

SUMMARY

Vermeulen et. al (2014) found many deep and stable scour holes in sharp bends along the Mahakam River in Indonesia. Understanding where they may develop, how deep they can become and why they remain stable is important for the safety of buried infrastructure and buildings near the river banks. However, the current knowledge is unable to explain the cause of the observed characteristics in scour holes of sharp bends. Therefore, we studied three hydrodynamic processes, which are in balance with each other and related to the scouring of the river bed. Previous studies also paid attention to some of these processes, but did not investigate how they relate to each other.

For our quantitative study, we used field measurements obtained in a sharp bend of the Mahakam River. The scour hole in this sharp bend is representative for other scour holes found in the river. The data was collected with an Acoustic Doppler Current Profiler at seven transects around the scour hole. We processed the collected data in such way, that we could calculate the terms in the Reynolds Averaged Navier Stokes equations. In this set of three momentum balances, we find the three hydrodynamic processes of interest: accelerations, pressure gradients and turbulent stress gradients.

Vermeulen (2014) used the field measurements as input for a simulation of the processes in the sharp bend with a hydrodynamic model. We used the model output as second dataset in our study. We processed the data in such way that we could evaluate the hydrodynamic processes along the whole bend. Therefore, we transformed the curved coordinate system into rectangular coordinates, which made it easier to compare the processes at different locations along the bend. A comparison between the two datasets revealed that the hydrodynamic model underestimates the plunging pattern of the flow, and overestimates the turbulent stresses in the scour hole.

In our study about the dominant hydrodynamic processes in scour holes of sharp bends, we first checked if we could assume an inviscid flow as suggested by Vermeulen et al. (2015) and Niesten (2016). They based their suggestion on the observation of non-hydrostatic pressure and vertical flow accelerations in scour holes. Therefore, Niesten proposed a method to obtain the non-hydrostatic pressure from such flow accelerations. However, she did not include turbulent stresses in her equation. We used the field measurements and the model output to validate her equation and showed that the underlying assumptions fail. The normal turbulent stress must be included in the equation to get a reliable approximation of the non-hydrostatic pressure head.

Next, we showed how the acceleration, pressure gradient and turbulent stress gradient behave along the sharp bend and how they change in the scour hole. In the streamwise and transverse momentum balance, the dominant terms upstream and downstream of the scour hole are the acceleration and the pressure gradient. In the scour hole, the turbulent stress gradient increases and reaches the same values as the other two processes. In the vertical momentum balance, the pressure gradient and the turbulent stress gradient show a huge increase in the scour hole and become more than 6 times larger than the acceleration. Therefore, we concluded that the assumption of inviscid flow fails in the scour hole.

A detailed evaluation of the processes in the vertical momentum balance revealed that the large increase of the turbulent stress is mainly covered by the vertical normal stress. This term originates from the variance in vertical flow velocity. Because there is no vertical flow at the water surface and the river bed, the velocity variance is also zero there. The largest variances were found around mid-depth in the deepest part of the scour hole. Therefore, we found large vertical gradients of the normal stress in the scour hole. This may explain why the normal stress shows such a huge increase.

In the discussion, we showed that the choices we made in processing the data, did only have small impact on our results. On the other hand, the differences between the field measurements and the model output may be more important. The underestimation of the vertical flow velocities and the overestimation of the turbulent stresses may have caused an invalid rejection of the inviscid flow assumption in the streamwise and transverse momentum balance. In the vertical momentum balance, the turbulent stress gradient remains dominant, even when we take the differences between the field measurements and the model output into account.

Therefore, we suggested that the large increase of the turbulent stresses in the scour hole is important to understand the processes related to scouring of the river bed. However, we recommend to study possible methods to make a reliable approximation of the velocity variances from field measurements and use these values to calibrate the hydrodynamic model again. If the hydrodynamic model gives better values of the turbulent stresses, our findings will probably somewhat change, but they will also be more useful in increasing our understanding of the processes related to scour holes in sharp bends.

CONTENTS

1	Introduction	1
1.1	Research topic	1
1.2	Knowledge gap	3
1.3	Research questions	3
1.4	Study area	4
1.5	Thesis outline	5
2	Background	7
2.1	Hydrodynamic characteristics	7
2.2	Reynolds Averaged Navier Stokes	11
2.3	Data collection	12
3	Methods	17
3.1	Processing field measurements	17
3.2	Processing model output	18
3.3	Non-hydrostatic pressure	20
3.4	Hydrodynamic processes	22
4	Results	25
4.1	Model reliability	25
4.2	Non-hydrostatic pressure	27
4.3	Hydrodynamic processes	31
4.4	Vertical momentum balance	37
5	Discussion	41
5.1	Data processing	41
5.2	Model reliability	45
5.3	Physical interpretation	47
6	Conclusions	55
	References	57
	Appendices	61
A	Local balances	61
B	Extensive balances	64

1 INTRODUCTION

In the first chapter, we introduce the research topic of the thesis. We explain the phenomenon of scour holes in sharp bends and why it is important to understand the hydrodynamic processes that specific river section. Next, we show what we already know about these processes and where we find a knowledge gap. Based on this knowledge gap we define some research questions, which we aim to answer in this study. Thereafter, we present the area that will be used to study the hydrodynamic processes in scour holes of sharp bends. Final, we explain the thesis outline.

1.1 Research topic

In the middle and lower course of a river, the channel shows often a mild slope and a meandering pattern. The curvature of these bends is usual mild, with the largest flow velocities in the outer bend and the smallest in the inner bend. Sedimentation patterns are related to these flow velocities, which results in deposition in the inner bend and erosion in the outer bend. Therefore, meanders have an asymmetric channel geometry, with a pool in the outer bend and a bar in the inner bend (figure 1.1) (Ottevanger, 2013), (Vermeulen, 2014).

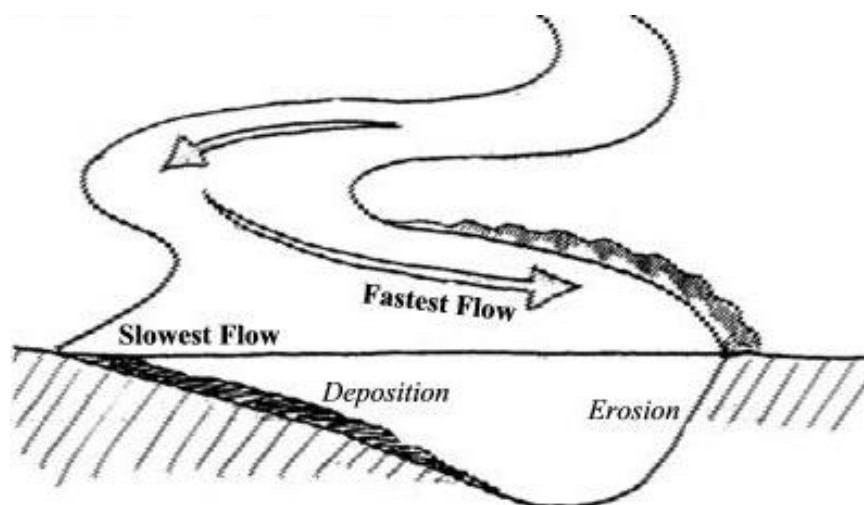


FIGURE 1.1 - TYPICAL ASYMMETRIC MEANDER BEND PROFILE (KOH, 2011)

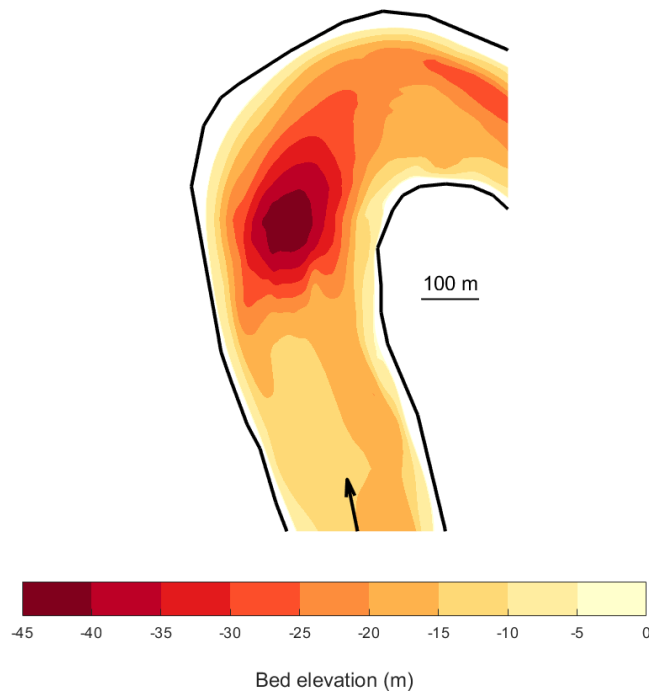


FIGURE 1.2 - CHANNEL BATHYMETRY OF A SHARP BEND WITH A DEEP SCOUR HOLE

Sometimes, the curvature of a meander increases, which makes the bends remarkable sharp. In such sharp bends, deep scour holes may be found (figure 1.2) (Vermeulen, 2014). Scour holes can be identified by a local, abrupt and relatively large drop of the bed elevation. Such scour holes originate from a local increase of the bed shear stress. If the bed shear stress passes a critical value, erosion may exceed deposition. This results in scouring of the river bed, until erosion and deposition are in equilibrium again (MacVicar & Rennie, 2012).

Human-made constructions, like bridge pillars or weirs, are often a cause of a local increase in bed shear stress (Tan, et al., 2005). These constructions interrupt the flow field, which results in flow accelerations, gradients in turbulent stresses and a corresponding increase of the bed shear stress. However, in the case of sharp bends, human-made constructions do not play a role. Therefore, we call this phenomenon autogenic scour. Despite no external factors influence the scouring processes, such autogenic scour holes may result in an increase of the water depth by a factor 3 (Vermeulen, et al., 2015), which has a large impact on the local channel geometry.

Knowing the cause of scour hole formation and why scour holes remain stable is crucial for companies associated with the construction of buried infrastructure. Pipelines, which transport for example oil and gas, should always remain below the river bed to prevent damage by strong currents or objects carried with the flow. Destruction of the pipes can result in serious economic and ecological consequences. Therefore, the companies must know where scour holes can develop and what depth they may reach (Sawatsky, et al., 1998), (Fassnacht & Conly, 2000), (Belatos, et al., 2011).

Another reason why understanding scour hole development is important, is river bank stability (Klingeman, et al., 1984), (Huismans, et al., 2016). Scour holes cause a deepening of the river bed, which often results in an increase of the bank slope. A steep sloped river bank is often less stable, than a bank with a mild slope. Therefore, knowing where scour holes may develop and how large they can become, may provide essential information for people or companies who own buildings close to the river. They may use this knowledge to decide whether bank protection should be constructed.

1.2 Knowledge gap

Although it is clear that it is important to understand the processes related to scour hole formation and stability in sharp bends, there is a lack in knowledge about this phenomenon (MacVicar & Rennie, 2012), (Vermeulen, et al., 2015). In the case of scour due to human-made constructions, we are able to explain the processes. However, if we have to deal with autogenic scour, as observed in sharp bends, our current understanding is still limited to a description of observed hydrodynamic processes.

Changes in hydrodynamic processes influence the magnitude of the bed shear stress, which makes them an important factor to understand bed scour. We may define three hydrodynamic processes in a river: flow, pressure and turbulence. These three processes are in balance with each other, which means that a change of one of them immediately is balanced by another. The gradients that are caused by these changes may be used as indicator for the magnitude of the change in bed shear stress (Fox, et al., 2011).

Previous studies showed that each of the three hydrodynamic processes change around scour holes in sharp bends. Vermeulen et. al (2015) revealed an increase of the near-bed velocity in the downstream part of the scour hole, which resulted in flow accelerations along the scour hole. They also observed deviations from a hydrostatic pressure distribution, which causes a gradient in pressure. Niesten (2016) observed the same patterns in another sharp bend with a deep scour hole. In both studies, the authors suggest that the pressure gradient balances the flow accelerations. However, they did not investigate the role of turbulent stress gradients.

MacVicar and Rennie (2012) studied autogenic scour in a straight channel. They observed an increase of the turbulent stress in the scour hole. The largest increase was found around the location where the water enters the scour hole. They had not enough information to explain the cause of scour hole formation, but they suggest that turbulent stress gradients may be the dominant factor. However, they did not compare the gradients in turbulent stresses with flow accelerations and the pressure gradient. Therefore, we only know that scour holes cause a change in each of the three hydrodynamic processes, but we cannot explain how these processes relate to each other.

1.3 Research questions

An important step in improving our understanding about scour hole formation and stability, is a study about the three hydrodynamic processes in scour holes of sharp bends. First, we will determine if the suggestion made by Vermeulen et al. (2015) and Niesten (2016) about negligible turbulent stresses (often called inviscid flow), is correct. Next, we will evaluate how the hydrodynamic processes behave around the scour hole. We will try to explain the observed patterns, and determine which processes are dominant.

“Which hydrodynamic processes are dominant in scour holes of sharp bends?”

1. May the hydrodynamic processes be described with the assumption of inviscid flow?
 - 1.1. Does the balance of hydrodynamic processes support the assumption of inviscid flow?
 - 1.2. What may explain the correctness or incorrectness of the inviscid flow assumption?
2. How do the hydrodynamic processes behave and relate to each other in a scour hole?
 - 2.1. How do scour holes in sharp bends change the behavior of hydrodynamic processes?
 - 2.2. Can we obtain one or more dominant processes around the scour hole?



FIGURE 1.3 - STUDY AREA WITH THE SHARP BEND OF INTEREST (C) NEAR THE KUTAI LAKES (B) IN THE INDONESIAN PROVINCE EAST-KALIMANTAN (A) (GOOGLE MAPS)

1.4 Study area

For the study about the hydrodynamic processes in scour holes of sharp bends, we will use a dataset collected by Vermeulen (2014) in a sharp bend of the Mahakam River in Indonesia (figure 1.3c). The Mahakam River is located on the Indonesian island Borneo, in the province East-Kalimantan (figure 1.3a). From the mountains of Borneo in the west, the river flows via the Kutai lakes (figure 1.3b) towards the Mahakam Delta (Vermeulen, 2014). The average discharge of the river is about $3000 \text{ m}^3/\text{s}$, the catchment has an area of 77150 km^2 and the river has a mild slope, which is also visible by the meandering topography. The average width of the river is 300 meters, the average depth is about 15 meters (Vermeulen, et al., 2014).

Along the Mahakam River, many sharp bends with deep scour holes are located. Within the observed river length of 200 km, 35 deep scour holes were found. These scour holes have a depth which is at least 3 times larger than the average depth. The scours are located at a distance of half a river width upstream of the point of highest curvature in a bend. The river cross-section at the scour holes is often symmetric, with the deepest point in the river center. This is in contrast with the asymmetric profile found in mildly curved bends (figure 1.1). So, in sharp bends with a scour hole, no point bar will develop (Vermeulen, et al., 2014).

The sharp bend that will be investigated in this study, lies in the Kutai basin (figure 1.3b). This sharp bend is representative for the many other sharp bends found in the Mahakam River. In the sharp bend, a deep scour hole is located (figure 1.2). The scour hole has an upstream slope of 11° and a downstream slope of 5° . The width at the bend is a bit larger than the average width, but the depth shows a huge increase up to more than 40 meters, which will cause the cross-section to become 3 times larger than average (Vermeulen, et al., 2015).

1.5 Thesis outline

In chapter 2, we give some theoretical background about the concepts and equations used throughout the thesis. We present the hydrodynamic characteristics of scour holes in sharp bends, introduce the most important equations and explain how the used data was collected. Next, chapter 3 presents the methods used to answer the research questions. We explain how we processed the raw dataset to get terms which could be used to quantitatively evaluate the hydrodynamic processes. Thereafter, we explain how we modified the basic equations to make them suitable for our study.

In chapter 4, the results of the study are presented. First, we show the reliability and limitations of our dataset. Then, we continue with the results of the study towards the correctness of the inviscid flow assumption. Thereafter, we present an evaluation of the hydrodynamic processes around the scour hole. We discuss the presented results in chapter 5. We show how the results may change, if we made other choices in the processing of the data. Next, we discuss the reliability of our dataset. Final, we discuss the physical meaning of our results. In chapter 6, we present the conclusions of our study.

2 BACKGROUND

Before we continue with a description of the methods, we present the theoretical background which is required to understand the next chapters. First, we explain the hydrodynamic characteristics of river bends and scour holes. This knowledge may be used to interpret the results later. Then, we present the Reynolds Averaged Navier Stokes equations, which are used for the quantitative analysis of the balance in hydrodynamic processes. Final, we explain how the data was collected in the sharp bend of the Mahakam River.

2.1 Hydrodynamic characteristics

We will study the hydrodynamic processes in scour holes of sharp bends. Both sharp bends and scour holes change the flow, pressure and turbulent stresses compared to a straight river. Therefore, it is important to be able to distinguish their contribution to these changes and to know how they interact. We briefly discuss the differences between 'normal' and sharp bends, and continue with the hydrodynamic characteristics of scour holes. Next, we explain the interaction between sharp bends and scour holes, in the case they are observed in the same river section.

2.1.1 River bends

Flow in a bend is influenced by two major forces: the centrifugal acceleration and the centripetal pressure gradient. When water enters a bend, the curvature initiates a centrifugal acceleration. This force pushes the water near the surface towards the outer bend (figure 2.1a) (Blanckaert, et al., 2013). The result is an increase of the water level in the outer bend and a decrease in the inner bend, which is called superelevation. The centrifugal forces, which bring extra water towards the outer bend, must be compensated in some way to prevent an infinite increase of water and corresponding flooding. The force that provides this required balance is known as the centripetal pressure gradient (figure 2.1b) (Nanson, 2010), (Ottevanger, 2013). A local imbalance between the centrifugal acceleration and the centripetal pressure gradient (figure 2.1c) is required to initiate a secondary spiral flow (figure 2.1d) (Blanckaert & Vriend, 2004), (Corney, et al., 2006).

Because of the outward directed secondary flow near the water surface, the main velocity core shifts towards the outer bend and changes the channel geometry. Bed shear stress and

corresponding sedimentation patterns are directly related to the flow velocity magnitude. If the bed shear stress passes a critical value, erosion will start. If it remains below that value, sediments might deposit (Fox, et al., 2011). When the main velocity core is pushed towards the outer bend, the bed shear stress will also increase in that river section. On the other hand, velocities in the inner bend will decrease, and so does the bed shear stress. The result is erosion in the outer bend, and deposition in the inner bend, which finally leads to an asymmetric channel with a pool in the outer bend and a point bar in the inner bend (figure 2.2).

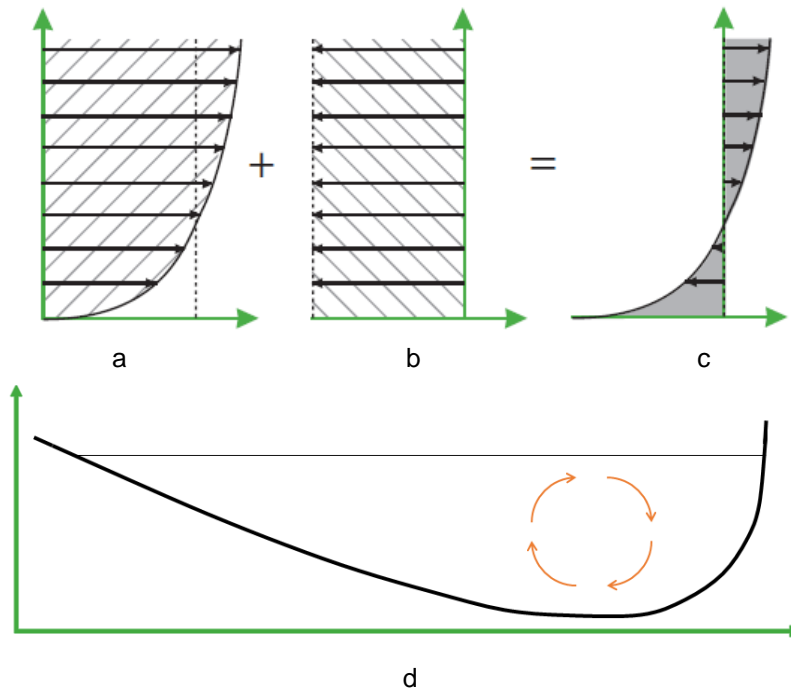


FIGURE 2.1 - LOCAL IMBALANCE (C) BETWEEN THE CENTRIFUGAL ACCELERATION (A) AND THE CENTRIPETAL PRESSURE GRADIENT (B) IN AN ASSYMETRIC CROSS-SECTION OF A RIVER BEND RESULTS IN A SECONDARY FLOW (D) (OTTEVANGER, 2013)

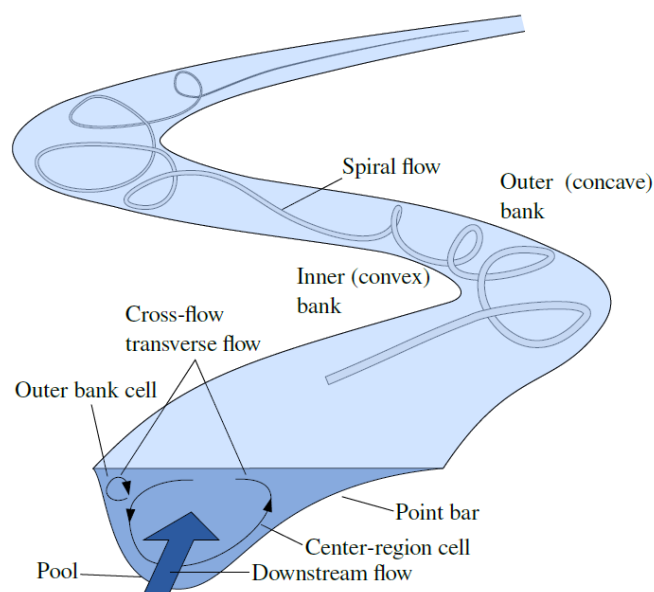


FIGURE 2.2 - SPIRAL FLOW THROUGH MEANDERING CHANNEL (VERMEULEN, 2014)

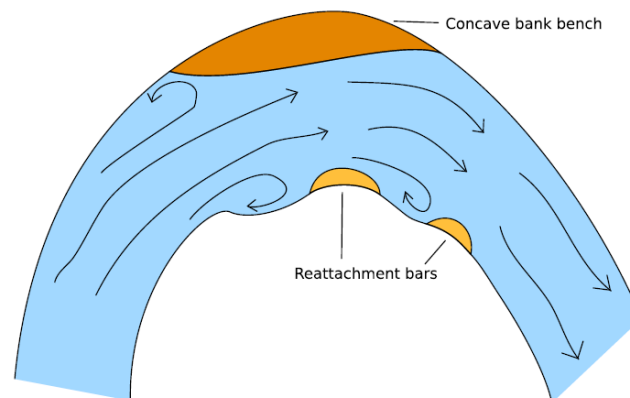


FIGURE 2.3 - REATTACHMENT BARS AND CONCAVE BANK BENCH IN SHARP BENDS (VERMEULEN, 2014)

2.1.2 Sharp river bends

The hydrodynamic characteristics of 'normal' (or mild) bends, show some differences with sharp bends. As the study is about scour holes in sharp bends, it is important to understand these differences. In sharp bends, the pattern of erosion in the outer bend and deposition in the inner band reverses (Vermeulen, et al., 2014). The banks in the outer bend become stable, and a concave bank may develop. In the inner bend, no point bar is visible, but some small reattachment bars (figure 2.3).

The cause of this changed erosion a deposition pattern may be explained from the flow processes in sharp bends. In sharp bends, secondary flow cells are a dominant hydrodynamic process, while in mild bends they may be negligible (Crosato, 2008), (Ottevanger, et al., 2012). The main secondary flow cell causes a redistribution of the flow, which results in the asymmetric cross-section. The outer bank cell, however, rotates in opposite direction (figure 2.2). Therefore, the outer bank cell reduces the shear stress and so the erosion of the outer bank in sharp bends (Blanckaert & Vriend, 2010), (Blanckaert, 2011).

2.1.3 Scour holes

Scour holes can be identified by a local, abrupt and a relatively large drop of the bed elevation. Scour holes can be found around human-made constructions (Tan, et al., 2005), in bedrock canyons (Venditti, et al., 2014), in a riffle-pool structure (Schnauder & Sukhodolov, 2012), close to overbank flows (Alford, et al., 1982), in a river with large ice jams (Beltaos, et al., 2012), and in sharp bends (Vermeulen, et al., 2014).

Because of the drop of the bed level, a scour hole causes a large and local increase of the channel cross-section. This will directly change the flow field and results in an increase of the water surface level. The total discharge in a river equals the product of the average flow velocity and the cross-sectional area (Fox, et al., 2011). The increase in cross-sectional area results in a decelerating flow where the water enters the scour hole. Around the deepest part of the scour hole, the maximum velocity core, which is usually near the water surface, is spread over the whole depth (figure 2.4).

When the flow leaves the scour hole, an acceleration is visible, with a peak in velocity near the bed (Vermeulen, et al., 2015). Previous studies revealed that the flow near the water surface continues to decelerate in the downstream part of the scour hole, even when the cross-sectional area becomes smaller. This result in a reversed flow velocity field at the downstream end of a scour hole, with largest velocities near the bed (MacVicar & Rennie, 2012), (Fazlollahi, et al., 2015).

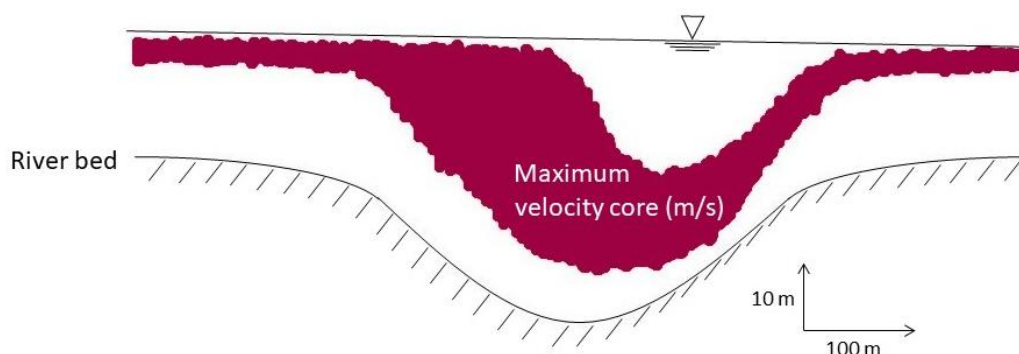


FIGURE 2.4 - LOCATION OF MAXIMUM VELOCITY CORE AROUND A SCOUR HOLE

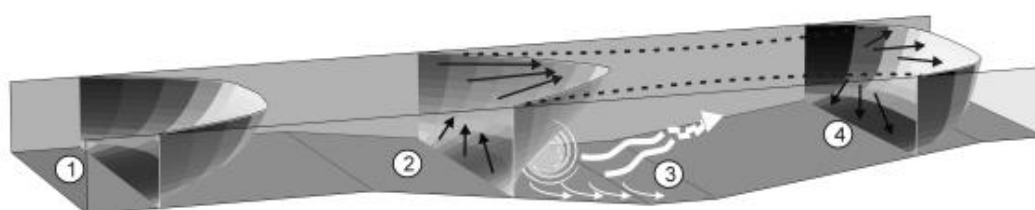


FIGURE 2.5 - CONCEPTUAL MODEL OF FLOW (BLACK ARROWS) AND TURBULENCE (WHITE ARROWS) IN A SCOUR HOLE (MACVICAR & RENNIE, 2012)

The increase of the near-bed velocities may be important for the morphological stability of the scour hole. Usually, the decrease of flow velocity, due to an increase of the cross-sectional area, will make the bed shear stress small (Fox, et al., 2011). This supports deposition of sediments, which finally results in filling up of the hole. However, the increased near-bed velocities make the bed shear stress large enough to prevent deposition in the downstream part of the scour hole (Venditti, et al., 2014).

At the entrance of the scour hole, the near-bed velocities are not large enough to prevent deposition. They decrease in this area, because the flow is not capable of following the bed level. Therefore, there may be flow separation near the river bed in the upstream part of the scour hole. This causes an increase of the turbulent stresses, which makes the bed shear stress large enough to prevent deposition. So, the increase of bed shear stress in the upstream end of a scour hole is associated with turbulence (figure 2.5) (MacVicar & Rennie, 2012).

2.1.4 Scour holes in sharp bends

When scour holes are observed in sharp bends, the described flow patterns interact with each other and result in a unique phenomenon. First, the combined effect of superelevation from curvature (figure 2.6a) and surface level increase as a compensation for the lower average flow velocity (figure 2.6b), will cause an increase of the water surface level along almost the whole outer bend (figure 2.6c) (Vermeulen, et al., 2015). The water surface elevation is directly related to the pressure (Fox, et al., 2011). Therefore, it is easy to determine a hydrostatic pressure gradient in streamwise and transverse direction from surface elevation maps (figure 2.6).

Second, the existence of the scour hole supports flow separation in the sharp bend. The large increase of the cross-section makes it easier for the flow to separate near the banks (figure 2.7) (Vermeulen, et al., 2015). Because the discharge remains the same, the flow velocity in the channel center will increase. An increase of the flow velocity will directly result in an increased bed shear stress, which prevents deposition of sediments. So, flow separation in bends may support the morphological stability of scour holes (Rhoads & Kenworthy, 1995), (Gharabaghi, et al., 2007).

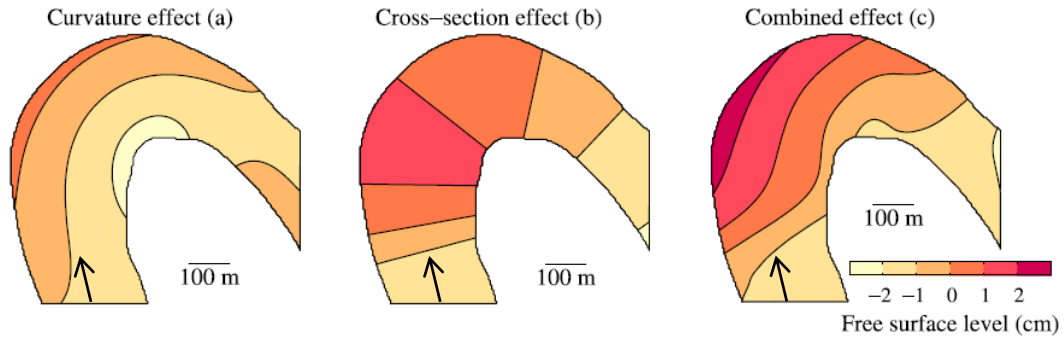


FIGURE 2.6 - DEVIATION FROM UPSTREAM WATER SURFACE ELEVATION AS RESULT OF THE CURVATURE (A), CROSS-SECTION INCREASE (B) AND THE COMBINED EFFECT (C) (VERMEULEN, ET AL., 2015)

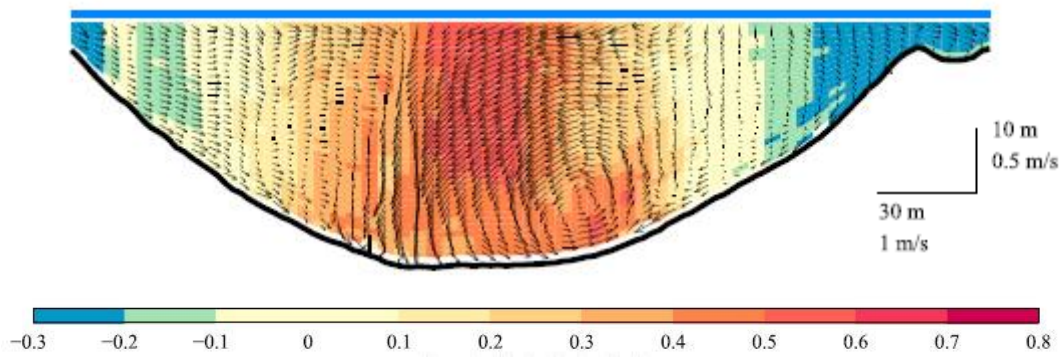


FIGURE 2.7 - STREAMWISE FLOW VELOCITY (COLORED SCALE - M/S) THROUGH CROSS-SECTION ABOVE A SCOUR HOLE (VERMEULEN, ET AL., 2015)

2.2 Reynolds Averaged Navier Stokes

In the quantitative analysis of the hydrodynamic processes around the sharp bend of interest, we will use the Reynolds Averaged Navier Stokes (RANS) equations. The Navier Stokes equations are a set of three differential equations which can be used to describe the flow of a fluid. The underlying theory of the equations is that a change of the impulse of a fluid particle (which results in an acceleration), is always balanced by a change in pressure and turbulent forces which act on that particle (Fox, et al., 2011). Therefore, these equations can be used to evaluate the relative contribution of the three hydrodynamic processes in the scour hole of the sharp bend.

As there are three equations, they can be used to describe a three-dimensional flow. Each of the three equations belongs to a total flow component u_T , v_T or w_T in a related direction; x , y or z . Flow in rivers is turbulent. Therefore, the total flow component in x -direction can be described with an average flow u and a deviation from that average flow u' . This way of describing a flow is called the Reynolds decomposition (Nieuwstadt, 1998).

$$u_T = u + u'$$

For the evaluation of the hydrodynamic processes, the average velocities from multiple time steps are used in the equations. As the mean flow component is a constant, its time-averaged component has the same value. The time-averaged fluctuating flow component equals zero. So, only the mean flow component is left after taking the average of all time steps. Therefore, the Navier Stokes equations reduce to the RANS equations, in which the flow components u , v and w express the mean flow.

The turbulent stresses in the RANS equations are expressed in normal σ and shear τ stresses. They origin from the variance between the fluctuating flow velocity components. In the case of normal stress, the changing fluctuations for each time step in a single direction are used to determine the variance. For the shear stress, the variance is calculated with the fluctuating velocities from two directions.

$$\sigma_{xx} = \rho \overline{u'u'} \quad \tau_{xy} = \rho \overline{u'v'}$$

In the RANS equations, the gradients of the three velocity components over time and in each of the three directions, are balanced by the pressure gradient and the turbulent stress gradients in three directions. This results in three momentum balances, in streamwise, transverse and vertical direction.

<i>Accelerations</i>	<i>Pressure gradient</i>	<i>Turbulent stress gradients</i>
$\frac{\partial u}{\partial t} + u \frac{\partial u}{\partial x} + v \frac{\partial u}{\partial y} + w \frac{\partial u}{\partial z}$	$= -\frac{1}{\rho} \frac{\partial p}{\partial x}$	$+ \frac{1}{\rho} \left(\frac{\partial \sigma_{xx}}{\partial x} + \frac{\partial \tau_{yx}}{\partial y} + \frac{\partial \tau_{zx}}{\partial z} \right)$
$\frac{\partial v}{\partial t} + u \frac{\partial v}{\partial x} + v \frac{\partial v}{\partial y} + w \frac{\partial v}{\partial z}$	$= -\frac{1}{\rho} \frac{\partial p}{\partial y}$	$+ \frac{1}{\rho} \left(\frac{\partial \tau_{xy}}{\partial x} + \frac{\partial \sigma_{yy}}{\partial y} + \frac{\partial \tau_{zy}}{\partial z} \right)$
$\frac{\partial w}{\partial t} + u \frac{\partial w}{\partial x} + v \frac{\partial w}{\partial y} + w \frac{\partial w}{\partial z}$	$= g - \frac{1}{\rho} \frac{\partial p}{\partial z}$	$+ \frac{1}{\rho} \left(\frac{\partial \tau_{xz}}{\partial x} + \frac{\partial \tau_{yz}}{\partial y} + \frac{\partial \sigma_{zz}}{\partial z} \right)$

We use the RANS equations in this thesis with SI-units.

u streamwise flow velocity (m/s)	x x -direction (m)
v transverse flow velocity (m/s)	y y -direction (m)
w vertical flow velocity (m/s)	z z -direction (m)
p pressure (kg/ms^2)	t time (s)
σ normal stress (kg/ms^2)	τ shear stress (kg/ms^2)
g gravity acceleration (m/s^2)	ρ fluid density (kg/ms^2)

2.3 Data collection

To make a quantitative evaluation of the hydrodynamic processes possible, we need a dataset with the terms in the RANS equations. The raw data was collected with an Acoustic Doppler Current Profiler along seven transects in the sharp bend of the Mahakam River (figure 2.8). An ADCP is usually attached below a boat, which sails slowly around the area of interest. ADCP's make use of the Doppler effect. The Doppler effect is the change of a sound pitch from relative displacement. The effect is similar to a passing train (Teledyne RD Instruments, 2006). When the train approaches, you can hear a higher sound than when the train moves away. The change in sound pitch is directly proportional to the speed of the train, so you can determine that velocity if you measure the sound.

The same principle is used to measure the flow velocity in water. ADCP's transmit a sound into the water, which is echoed back by small particles, like sediments or plankton. From the time it takes before the echoes of that sound can be heard, it can determine the location of the particles and calculate a corresponding velocity. The underlying assumption is that these scatters have the same velocity magnitude and direction as the water itself. However, the ADCP can only measure echoes in the same direction as it has send the sound, which is called radial motion. If scatters reflect the sound while moving perpendicular to the ADCP, the radial velocity will be zero. So, only the component parallel to the acoustic beam is measured (Teledyne RD Instruments, 2006).

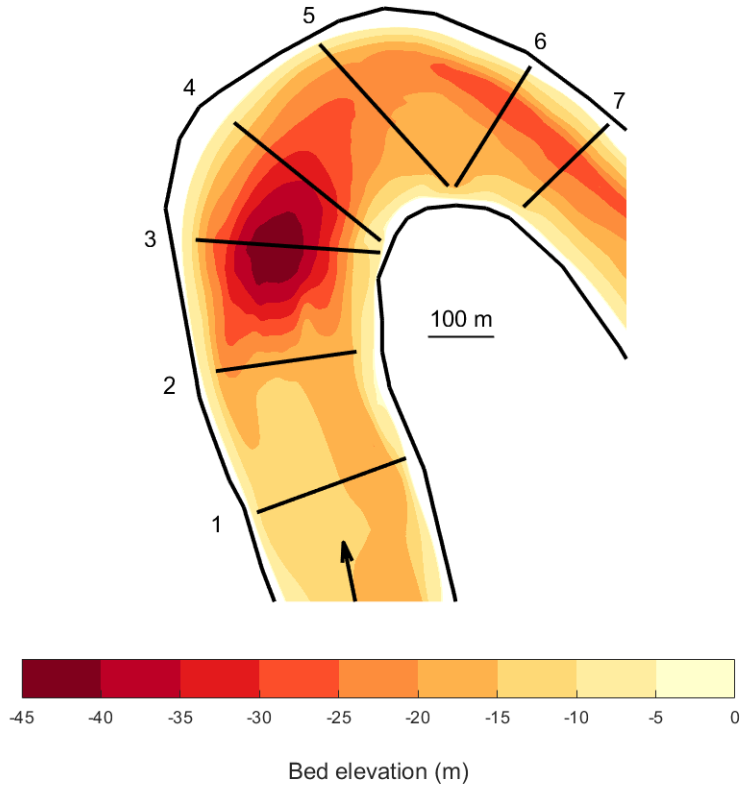


FIGURE 2.8 - LOCATION OF TRANSECTS IN SHARP BEND WHERE FLOW VELOCITIES WERE MEASURED

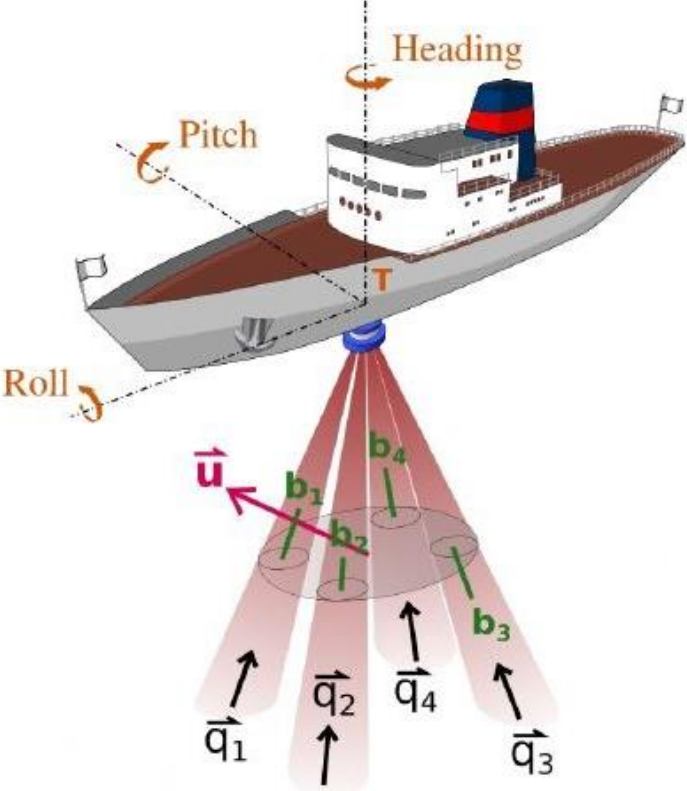


FIGURE 2.9 - TAKING VELOCITY MEASUREMENTS WITH AN ADCP BELOW A BOAT (VERMEULEN, ET AL., 2015)

Therefore, it is impossible to measure three-dimensional flow with a single sound echo. To make such measurements possible, the ADCP sends a sound in four different directions into the water, which is visible in four acoustic beams (figure 2.9). The radial velocities that are collected along these beams, are used to approximate the velocity components at a specific depth. An often-used assumption is homogeneous flow between the beams, so the velocities can be approximated throughout the whole measuring area (figure 2.10a). However, Vermeulen et al. (2015) showed that this assumption fails when the depth in a river becomes too large or if the river bed shows large variations.

The acoustic beams diverge with increasing depth (figure 2.10). So, the homogeneous assumed flow increases also with depth. In shallow rivers, this may not cause significant errors, but in rivers with large depths, the homogeneous flow assumption makes the data unreliable. Vermeulen et al. (2015) proposed a new method to obtain the flow velocities from the ADCP measurements. In the new method, the flow is assumed to be steady, so the velocities could be approximated from measurements at multiple time steps. This makes it possible to decrease the volume in which homogeneous flow is assumed (figure 2.10b). With this method, the velocity data in our study area was generated.

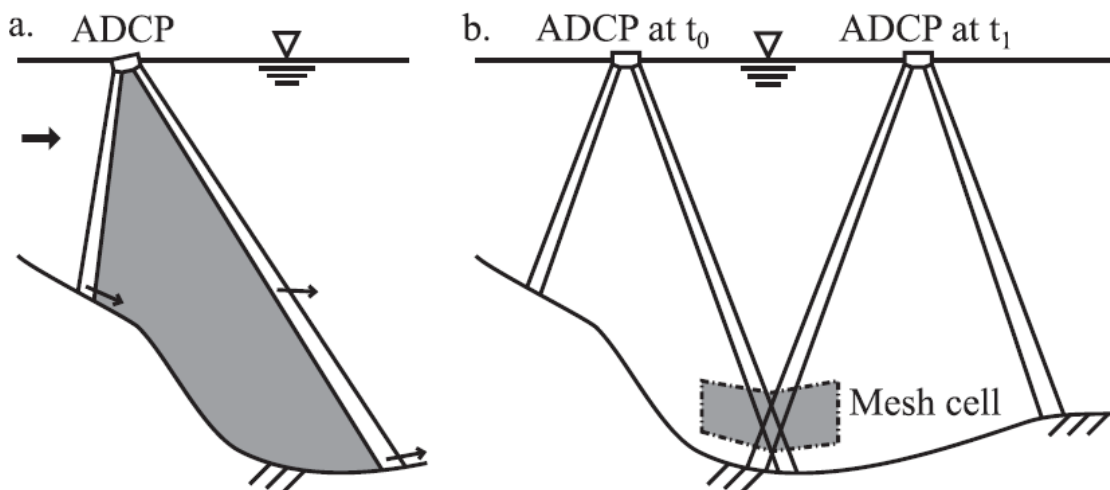


FIGURE 2.10 - FAILURE OF HOMOGENEOUS ASSUMPTION WITH INCREASING DEPTH AND CHANGING BED ELEVATION (VERMEULEN, ET AL., 2015)

Mesh transect 4

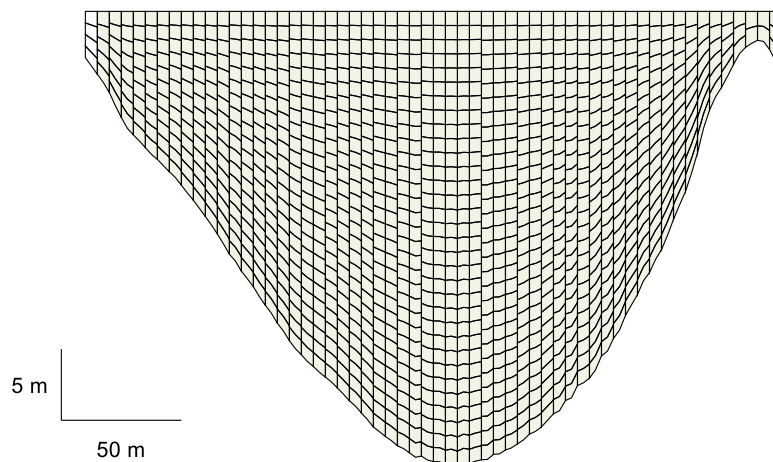


FIGURE 2.11 - MESH CELLS FOR PROCESSING VELOCITIES IN TRANSECT 4

The boat sailed 16 times along each transect, to collect the beam velocities in the sharp bend of the Mahakam River. Repeated measurements make it possible to distinguish mean and turbulent flow, which is important for our study (Vermeulen, et al., 2015). Based on the location of measurement, the beam velocities were assigned to a mesh cell (figure 2.11). The width of the mesh cells is taken constant, the height differs per cell to ensure each cell has about the same amount of beam velocities. Moreover, the cells must follow the channel bathymetry, which may cause a changing height for a single cell, especially near the bottom. The beam velocities within a mesh volume were corrected for heading, pitch and roll (figure 2.9), before they were used to calculate the mean velocity vector and the required three-dimensional velocity components.

3 METHODS

In the third chapter, we present the methods used to obtain our results. First, we explain how we processed the raw data to achieve the terms in the RANS equations. We also explain how the field measurements were used to make a hydrodynamic model of the sharp bend, and how we used the model output to estimate the terms in the RANS equations. Next, we present a method to check if we may use the same arguments as done by Vermeulen et. al (2015) and Niesten (2016) to assume inviscid flow. Final, we explain the methods which will be used to evaluate the hydrodynamic processes around the scour hole.

3.1 Processing field measurements

With the ADCP, a large dataset was collected in the sharp bend of interest. However, we did not need the whole dataset, only the data required to calculate the terms in the RANS equations is interesting for our study. The used data consists of 3 velocity components u , v and w , the variance between that velocities, x , y and z -coordinates and the number of beam velocities per mesh cell (figure 2.11), in each of the 7 transects. The constant width of the mesh cells is chosen to be 5 meters, the height differs around 1 meter.

For each transect a unique coordinate system was defined, based on the direction of the transects (figure 3.1a). If we observe the cross-section of a transect as a surface (as visible in the mesh (figure 2.11)), we define the streamwise flow velocity u and corresponding x -direction perpendicular to this surface, with a positive sign in downstream direction. The transverse velocity v and y -direction are horizontal in the surface, and positive towards the outer bend. The vertical velocity w and z -direction are vertical in the surface, and positive towards the water surface. The velocity components from the raw dataset were corrected according to these definitions, to achieve the velocity components in each transect.

Based on the corrected velocity components and the number of beam velocities per cell, we could determine the velocity variance. These variances may be used to calculate the normal and shear stresses. However, the variances were largely influenced by instrument noise, which makes the measured variance an unreliable indicator for the turbulent stresses. In the results, we show how the noise influences the approximation of the velocity variance.

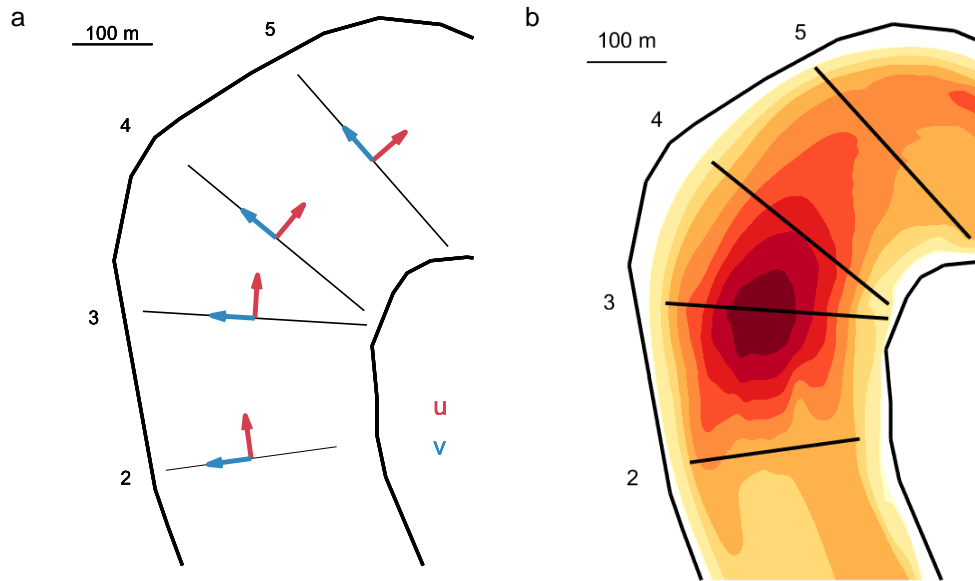


FIGURE 3.1 - FLOW DIRECTIONS (A) AND BED ELEVATION (B) AT THE TRANSECTS IN SHARP BEND

Not only the three-dimensional velocity components are required as input in the RANS equations, we also need the velocity gradients. The derivative in x -direction was determined from all beam velocities in a single mesh cell. Most cells contain about 200 beam velocities, from which an average velocity was calculated and interpolated to the transect. Some of beam velocities were measured upstream of the transect, and some downstream. The location of the measured beam velocities was used to determine the gradient in x -direction for a mesh cell.

In y and z -direction, the derivatives were determined from their neighboring cells. The difference between the averaged and interpolated velocity component in these cells, gives a more reliable estimation of the velocity gradient than in the method used for calculating the derivatives in x -direction. The reason for this improved reliability can be found in the number of used beam velocities, which is larger when the calculation is based on two mesh cells instead of one. Because the distance between the transects is large, the calculation of the x -derivatives could only be done within a single mesh cell.

3.2 Processing model output

Vermeulen (2014) used the measured data along the 7 transects of the sharp bend was to make a simulation of the flow in the sharp bend. The channel bathymetry, as measured by the ADCP, was used as a fixed boundary, just like an upstream inflow of $1700 \text{ m}^3/\text{s}$ and a downstream water level. The model could simulate a free surface, which is presented by the piezometric head h in the model output. This piezometric head can be expressed in terms of pressure p , density ρ , gravity acceleration g , and water depth z .

$$p = \rho g(h - z)$$

A large eddy simulation was used to model the turbulence. The turbulence was initialized by applying random velocity fluctuations to the constant inflow (Vermeulen, et al., 2015). For 100 different velocity fluctuations, a model run was performed. The output of each of that model runs, consist of 3 velocity components and a piezometric head at 365064 data points along the sharp bend. The average values of the 100 runs were used to determine the mean velocity components

and the flow derivatives. The differences between the 100 runs were used to determine the 6 velocity variances for each data point, which resulted after multiplication with the water density in the normal and shear stresses. As the 100 runs are not related to time, we cannot obtain the time derivative from the model output.

In the processing of the field measurements, we defined a unique coordinate system for each of the 7 transects. We used this method also for the model output and interpolated the simulated values to the same transects as in the field measurements, so we could compare the values. However, as we also want to evaluate the hydrodynamic processes along the whole bend, we need to compare the results between multiple transects, which is complicated if the coordinate system changes. Therefore, we transformed the model output to a new, and constant coordinate system, before we interpolated the data to the transects we want to evaluate. In the transformation of the model output, the channel bathymetry changes from a sharp bend (figure 3.2a) to a rectangular channel (figure 3.2b).

The transformed model output around the scour hole was interpolated to 800 transects, with a spacing of 1 meter. The mesh was chosen to be rectangular and constant, with the same values as used in the processing of the field measurements: 5 by 1 meters. The 3 velocity components and 6 velocity variances were interpolated to these transects, and afterwards corrected to achieve the values in the right direction. The piezometric head was also interpolated, but not correct, because the head is not related to a direction. The depth of each mesh cell was used to calculate the pressure from the piezometric head.

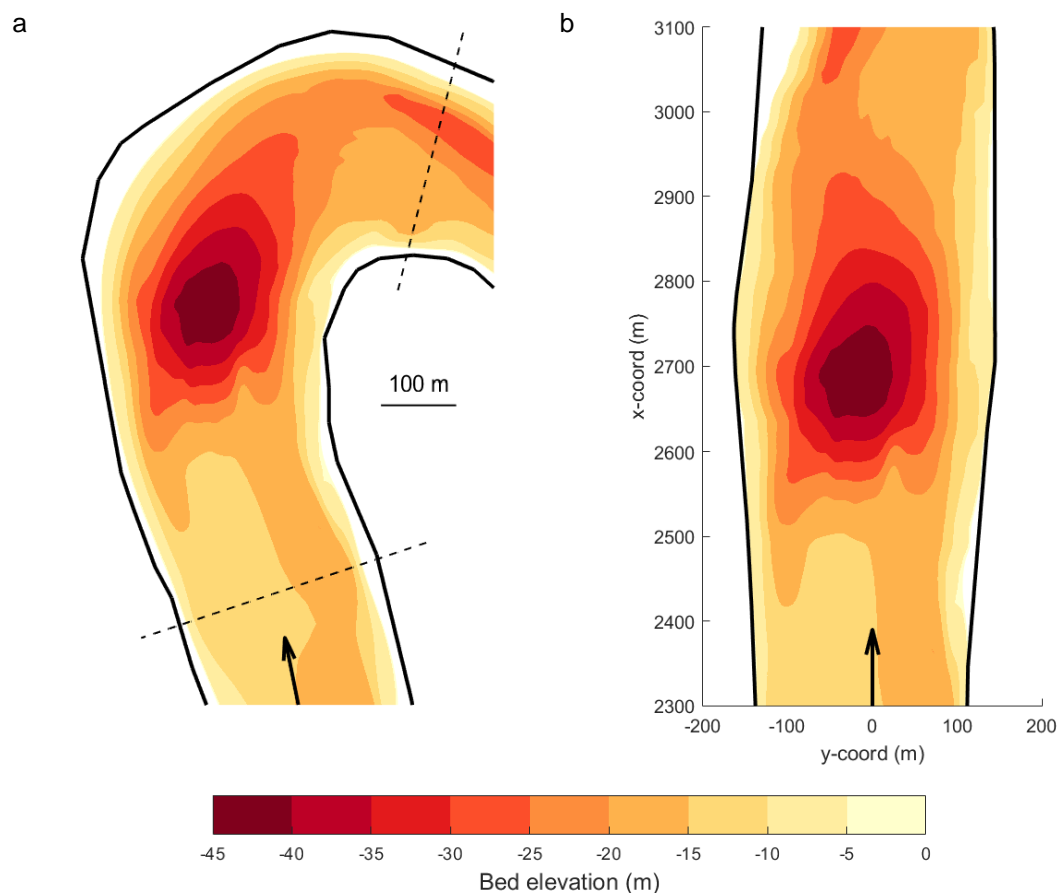


FIGURE 3.2 - TRANSFORMATION OF MODEL OUTPUT FROM CURVED (A) TO RECTANGULAR (B) COORDINATES

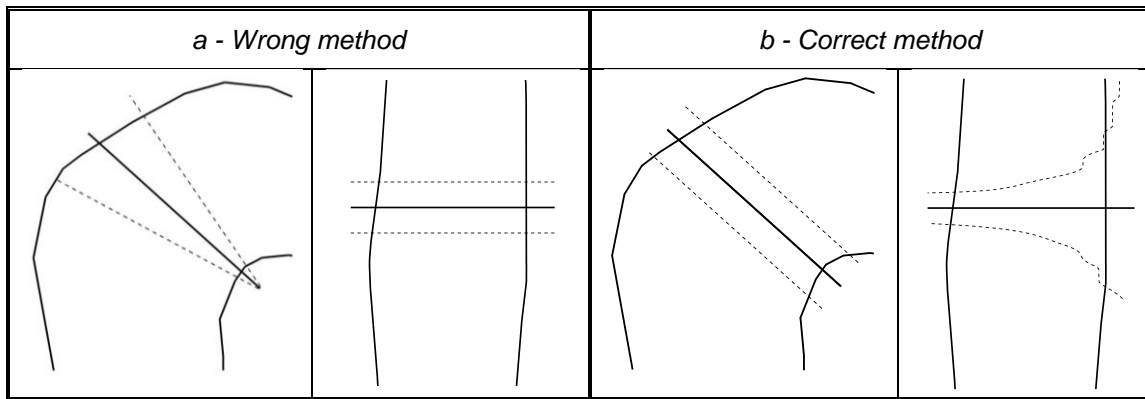


FIGURE 3.3 - WRONG (A) AND CORRECT (B) METHOD TO CALCULATE DERIVATIVES IN X-DIRECTION OF TRANSFORMED MODEL OUTPUT

The derivatives in y and z -direction were, just as with the field measurements, calculated from their neighboring cells. However, the derivatives in x -direction could not be calculated by this method, even if the spacing is only 1 meter. This is caused by the fact that a constant dx in the transformed data, originates from a changing dx in the original output (figure 3.3a). A dx of 1 meter in the transformed outer bend originates from a larger dx in the original output, while we see the opposite in the inner bend. So, calculating the gradients in x -direction from the transformed data, will give different kind of derivatives in the inner and outer bend, which makes a comparison of that values unreliable.

Therefore, we defined additional transects for the calculation of the derivatives in x -direction. For each of the 800 transects, we used its original coordinates to define an upstream and downstream transect at a constant distance of 2 meters in streamwise direction. Based on that coordinates, we defined 2 new transects in the transformed coordinate system. These transect show a small spacing in the outer bend and a large spacing in the inner bend (figure 3.3b). The velocities interpolated to the additional transects were used to calculate the derivatives in x -direction. We used the velocity difference between the additional upstream and downstream transect, but divided this value by the original constant dx . With this method, we expect to get a reliable approximation of the gradients in x -direction from the transformed model output.

3.3 Non-hydrostatic pressure

In a flow without flow accelerations and turbulent stress gradients, the pressure distribution reduces to a hydrostatic balance, in which the gravity acceleration balances the vertical pressure gradient. Deviations from this balance are always a result of flow accelerations and turbulent stress gradients. Vermeulen et. al (2015) and Niesten (2016) observed such deviations in deep scour holes of sharp bends. They also observed vertical flow accelerations in those scour holes. Therefore, they suggested that we may describe hydrodynamic processes in scour holes of sharp bends with an inviscid flow. However, they did not investigate the role of turbulent stress gradients.

Therefore, we will perform a detailed evaluation of the non-hydrostatic pressure around the scour hole, to check if the arguments to assume an inviscid flow retain in our case. Niesten proposed a method to obtain the non-hydrostatic pressure head from the vertical momentum balance. As she assumed an inviscid flow, she only included accelerations in her equation. She did not need model simulations and only used field measurements to obtain the non-hydrostatic pressure. We will validate her method with the piezometric head from the hydrodynamic model output. In the validation, we interpolate the model results to the same transects as in the field measurements. This allows us to compare the results from the field measurements with the model output.

We rewrite the pressure gradient of the vertical momentum balance in terms of hydrostatic p_h and non-hydrostatic pressure p_n . In the case of hydrostatic pressure, the vertical pressure gradient is constant and completely balanced by the gravity acceleration. Therefore, we can leave these terms out of the balance. This reduces the vertical momentum balance to an expression in which the flow accelerations and the turbulent stress gradients balance the non-hydrostatic pressure gradient. So, we can use this equation only to evaluate the non-hydrostatic pressure itself, not to compare it with its hydrostatic equivalent.

$$p = p_h + p_n$$

$$g - \frac{1}{\rho} \frac{\partial p}{\partial z} = g - \frac{1}{\rho} \frac{\partial p_h}{\partial z} - \frac{1}{\rho} \frac{\partial p_n}{\partial z} = -\frac{1}{\rho} \frac{\partial p_n}{\partial z}$$

$$\frac{\partial w}{\partial t} + u \frac{\partial w}{\partial x} + v \frac{\partial w}{\partial y} + w \frac{\partial w}{\partial z} = -\frac{1}{\rho} \frac{\partial p_n}{\partial z} + \frac{1}{\rho} \left(\frac{\partial \tau_{xz}}{\partial x} + \frac{\partial \tau_{yz}}{\partial y} + \frac{\partial \sigma_{zz}}{\partial z} \right)$$

To determine the non-hydrostatic pressure head, we must integrate over depth, from local depth z' to the free surface level η , which is equivalent to the piezometric head at the water surface h_s (figure 3.4). We divide the integration in two parts, distinguished by whether a term includes a derivative over z .

$$\int_{z'}^{h_s} \left(\frac{\partial w}{\partial t} + u \frac{\partial w}{\partial x} + v \frac{\partial w}{\partial y} - \frac{1}{\rho} \left(\frac{\partial \tau_{xz}}{\partial x} + \frac{\partial \tau_{yz}}{\partial y} \right) \right) dz + \int_{z'}^{h_s} \left(\frac{1}{2} \frac{\partial w^2}{\partial z} + \frac{1}{\rho} \frac{\partial p_n}{\partial z} - \frac{1}{\rho} \frac{\partial \sigma_{zz}}{\partial z} \right) dz = 0$$

We can directly obtain the result from the integration of the terms with a vertical gradient.

$$\int_{z'}^{h_s} \left(\frac{\partial w}{\partial t} + u \frac{\partial w}{\partial x} + v \frac{\partial w}{\partial y} - \frac{1}{\rho} \left(\frac{\partial \tau_{xz}}{\partial x} + \frac{\partial \tau_{yz}}{\partial y} \right) \right) dz + \frac{w^2}{2} + \frac{p_n}{\rho} - \frac{\sigma_{zz}}{\rho} = 0$$

We divide every term by the gravity acceleration g , to end up with an expression for the deviation from the hydrostatic pressure head in meters. We call this the “equation of Niesten”.

$$\frac{p_n}{\rho g} = -\frac{1}{g} \int_{z'}^{h_s} \left(\frac{\partial w}{\partial t} + u \frac{\partial w}{\partial x} + v \frac{\partial w}{\partial y} - \frac{1}{\rho} \left(\frac{\partial \tau_{xz}}{\partial x} + \frac{\partial \tau_{yz}}{\partial y} \right) \right) dz - \frac{w^2}{2g} + \frac{\sigma_{zz}}{\rho g}$$

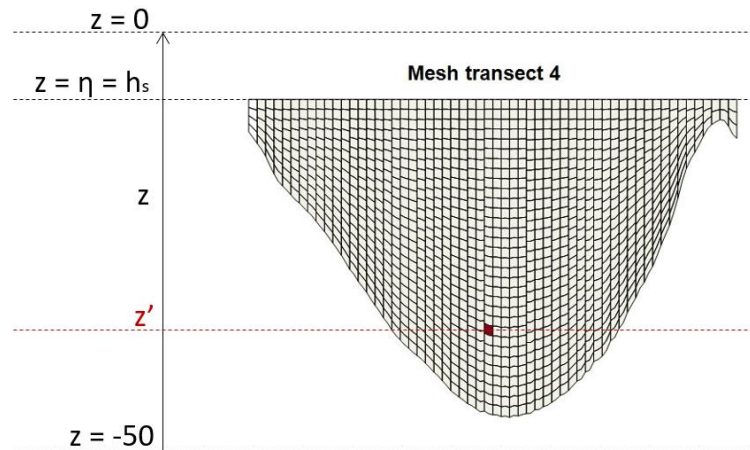


FIGURE 3.4 - DEFINITION OF TERMS IN THE INTEGRATION OF THE VERTICAL MOMENTUM BALANCE

In the output of the hydrodynamic model we find the piezometric head h throughout the whole bend. For the hydrostatic pressure, the head is constant over each column and the same as the free water surface level $\eta = h_s$. The heads at larger depths indicate a possible deviation from that hydrostatic head. To make a comparison with the obtained deviation from the hydrostatic head by the equation of Niesten possible, we define an expression to calculate the non-hydrostatic pressure head from the total head and the hydrostatic head.

$$p = p_h + p_n$$

$$\rho g(h - z') = \rho g(h_s - z') + p_n$$

$$p_n = \rho g(h - z') - \rho g(h_s - z')$$

$$\frac{p_n}{\rho g} = h - h_s$$

3.4 Hydrodynamic processes

A comparison between the non-hydrostatic pressure head from the equation of Niesten and the model output should reveal whether the arguments to assume an inviscid flow retain for our scour hole. However, if the arguments to assume inviscid flow turn out to be invalid, we may directly reject the assumption. The comparison is only based on a few transects around the scour hole and we did not take the streamwise and transverse momentum balance into account. Therefore, we need to use the model output to evaluate the hydrodynamic processes along the whole sharp bend, in each of the three momentum balances. This evaluation will reveal if we can make the assumption of inviscid flow. Moreover, it will provide insight in which processes are dominant around the scour hole.

To check the assumption of inviscid flow and to indicate which hydrodynamic processes are dominant, we will first evaluate the accelerations, pressure gradients and turbulent stress gradients along the scour hole. Therefore, we use the cross-sectional averaged absolute values of the three processes in the 800 interpolated transects. Using the absolute values prevents a reduced mean from both positive and negative values within a transect. The curves with the values of the three processes around the scour hole, will reveal for each balance if the assumption of inviscid flow can be done. The explained theory about the hydrodynamic characteristics of scour holes in sharp bends may help to understand why the balances support or reject the inviscid flow assumption.

<i>Acceleration</i>	<i>Pressure gradient</i>	<i>Turbulent stress gradient</i>
$\left u \frac{\partial u}{\partial x} + v \frac{\partial u}{\partial y} + w \frac{\partial u}{\partial z} \right $	$= \left -\frac{1}{\rho} \frac{\partial p}{\partial x} \right $	$+ \left \frac{1}{\rho} \left(\frac{\partial \sigma_{xx}}{\partial x} + \frac{\partial \tau_{yx}}{\partial y} + \frac{\partial \tau_{zx}}{\partial z} \right) \right $
$\left u \frac{\partial v}{\partial x} + v \frac{\partial v}{\partial y} + w \frac{\partial v}{\partial z} \right $	$= \left -\frac{1}{\rho} \frac{\partial p}{\partial y} \right $	$+ \left \frac{1}{\rho} \left(\frac{\partial \tau_{xy}}{\partial x} + \frac{\partial \sigma_{yy}}{\partial y} + \frac{\partial \tau_{zy}}{\partial z} \right) \right $
$\left u \frac{\partial w}{\partial x} + v \frac{\partial w}{\partial y} + w \frac{\partial w}{\partial z} \right $	$= \left -\frac{1}{\rho} \frac{\partial p_n}{\partial z} \right $	$+ \left \frac{1}{\rho} \left(\frac{\partial \tau_{xz}}{\partial x} + \frac{\partial \tau_{yz}}{\partial y} + \frac{\partial \sigma_{zz}}{\partial z} \right) \right $

In the streamwise and transverse momentum balance, we may divide the pressure gradient in a hydrostatic pressure gradient and a non-hydrostatic pressure gradient. As Vermeulen et. al (2015) and Niesten (2016) suggested that the non-hydrostatic pressure is important in scour holes, it is interesting to determine how its gradient behaves along the scour hole. Therefore, we compare the cross-sectional averaged value of the total pressure gradient, the hydrostatic pressure gradient and the non-hydrostatic gradient in the 800 interpolated transects.

$$\frac{1}{\rho} \frac{\partial p}{\partial x} - \frac{1}{\rho} \frac{\partial p_h}{\partial x} - \frac{1}{\rho} \frac{\partial p_n}{\partial x} = 0$$

$$\frac{1}{\rho} \frac{\partial p}{\partial y} - \frac{1}{\rho} \frac{\partial p_h}{\partial y} - \frac{1}{\rho} \frac{\partial p_n}{\partial y} = 0$$

Next, we will perform a more detailed evaluation of hydrodynamic processes in the balance which shows largest deviation from the inviscid flow assumption. In the river section upstream of the scour hole, the hydrodynamic processes may be well described with an inviscid flow (Fox, et al., 2011). When the water passes the scour hole, the turbulent stress gradients will probably increase and change the balances. We think that understanding these changes may be important to improve our knowledge about scour hole formation and stability. Therefore, a detailed study of the largest changes will contribute the most to reach this goal.

In this detailed study of the hydrodynamic processes, we will first extend the previous evaluation of the three processes to a balance in which each single term can be found. Again, we use the absolute values to prevent lower average values. From this balance, we can obtain which terms are dominant. Next, we will show the variation of these dominant terms within five cross-sections. The five cross-sections are chosen in such way that we can compare the dominance upstream, along and downstream of the scour hole (figure 3.5). A physical interpretation of the observed patterns may reveal in which direction we should do further study about the origin and stability of scour holes in sharp bends.

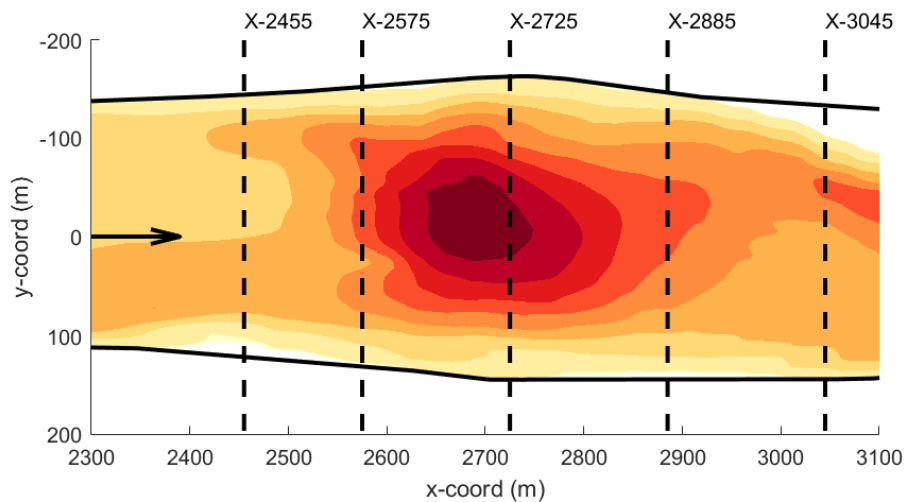


FIGURE 3.5 - LOCATION OF TRANSECTS WHICH WILL BE EVALUATED IN DETAIL

4 RESULTS

We present the results of our study about the hydrodynamic processes in scour holes of sharp bends. First, we use the field measurements to determine the reliability of the model output. We compare the estimated flow velocities and turbulent stresses from both datasets and explain the differences. Next, we check the suggestion made by Vermeulen et. al (2015) and Niesten (2016) about the relation between non-hydrostatic pressure and vertical flow accelerations. Thereafter, we show which hydrodynamic processes are dominant in each of the three momentum balances. Final, we explain the observed patterns in the vertical momentum balance in detail.

4.1 Model reliability

Before we present the results from the explained methods, we first study the reliability of the hydrodynamic model output. In obtaining the results, we will mostly use the output from the hydrodynamic model, which means that we assume the model simulations to be a reliable approximation of reality. A calibration of the model revealed that the simulations show indeed good agreement with the field measurements (Vermeulen, et al., 2015). However, there are some differences, which may be important for the interpretation of our results.

First, the model underestimates the plunging pattern of the flow into the scour hole. If we compare the vertical flow velocities in the field measurements with the model output, we find smaller values in the model output (figure 4.1b). In cross-section 3, the largest vertical flow velocities in the field reaches a value above 0.12 m/s, while the maximum downward vertical velocity in the model output does not exceed 0.08 m/s. The reversed pattern is observed in cross-section 4, where the maximum upward directed vertical velocity in the field measurements is 0.03 m/s larger than in the model output.

The underestimation of the plunging flow pattern is also visible in the streamwise flow velocity in the scour hole (figure 4.1a). Due to the smaller downward velocity in the model output, the maximum velocity core in cross-section 3 remains close to the water surface, while in the field measurements this core is spread over the whole depth. In cross-section 4, the field measurements show a reversed velocity distribution with the core near the bed. In the model simulations, such large near-bed velocities cannot be observed.

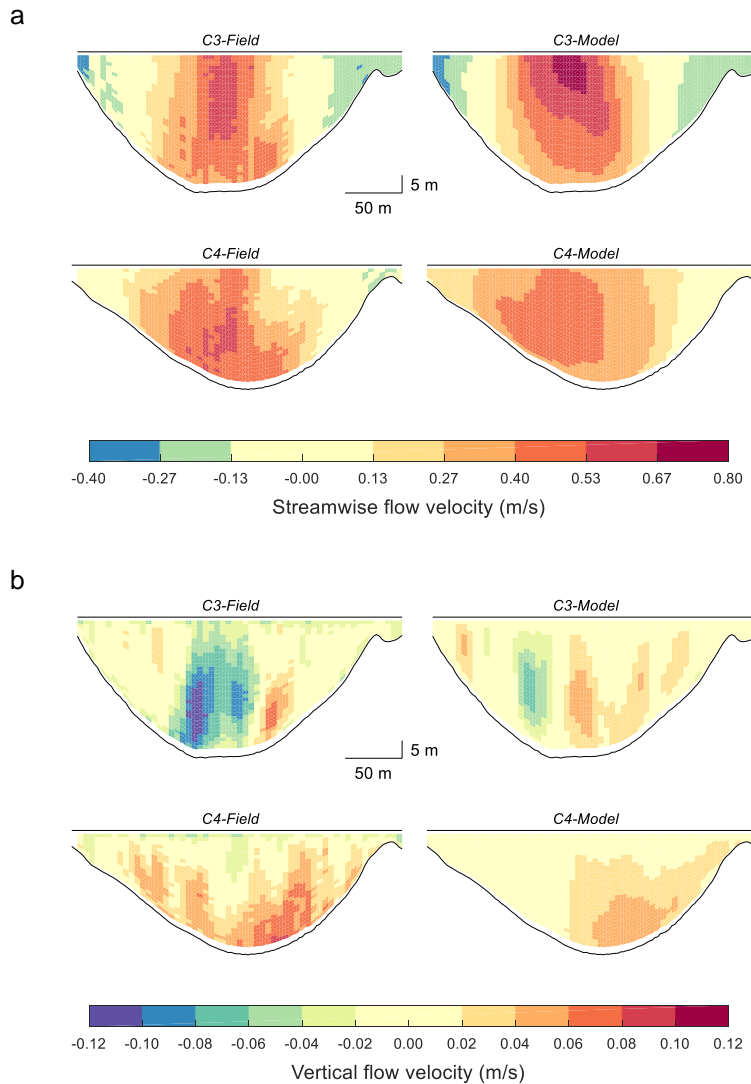


FIGURE 4.1 - UNDERESTIMATION OF STREAMWISE (A) AND VERTICAL (B) FLOW VELOCITIES IN SCOUR HOLE

Besides the flow velocities, we can also compare estimations of the normal and shear stresses from the field measurements with the model output. Unfortunately, such comparing is more complicated than in the case of flow velocities, because instrument noise is important here. The normal and shear stresses in the RANS equations origin in theory from velocity fluctuations in a turbulent flow. In obtaining field measurements with an ADCP, however, instrument noise may increase these fluctuations with an order of magnitude (Kim & Muste, 2012), (Vermeulen, et al., 2014). The instrument noise is largest for the velocity variances in streamwise and transverse direction, which makes an estimation of the normal stress in these directions unreliable. However, for the approximation of the other turbulent stresses, the instrument noise is less dominant and these stresses may be approximated with measured velocity variances (Nystrom, et al., 2007).

To get the approximations of the normal and shear stresses from the field measurements for a mesh cell, we must multiply the observed variance with the number of beam velocities in that cell. So, large differences between the number of beam velocities within a cross-section may have a large impact on the estimation of the variance. In cross-section 4, the number of beam velocities is most equally spread (figure 4.2). Therefore, we use this cross-section to compare the approximations of the turbulent stresses from the field measurements with the model output.

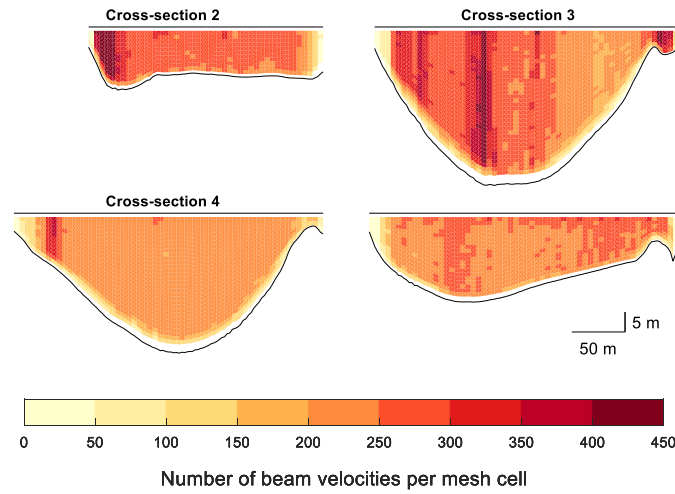


FIGURE 4.2 – SPREADING OF THE NUMBER OF BEAM VELOCITIES OVER THE CROSS-SECTIONS AROUND THE SCOUR HOLE

The results show indeed a difference of one order of magnitude between the measured normal stress in vertical (figure 4.3c) and the other two directions (figure 4.3a-b). The vertical normal stress and the three shear stresses (figure 4.3d-e-f) show much larger agreement between the measurements and the model output, the differences are mostly within an order of magnitude. However, the modelled stresses are larger than the measured stresses. Although the instrument noise is not dominant, there is probably always a small error which increases the velocity variances. Therefore, we should expect the measured stresses to be larger than the modelled stresses, but this is clearly not the case.

The larger stresses in the model output cannot be explained from larger vertical velocities in the model simulations, because they are larger in the field measurements (figure 4.1b). Therefore, the difference must be caused from an overprediction of the turbulence in the model simulations. The turbulence in the modelling was initialized by applying random fluctuations to the constant inflow. The variance between the 100 different velocity fluctuations was used to calculate the stresses. So, the initialized fluctuations seem to be chosen too large, which resulted in an overprediction of the turbulent stresses in the model output.

4.2 Non-hydrostatic pressure

Vermeulen et. al (2015) and Niesten (2016) suggested that deviations from the hydrostatic pressure head are caused by vertical accelerations, and used this relation to assume an inviscid flow in scour holes of sharp bends. Niesten proposed a method to obtain the non-hydrostatic pressure head, which resulted in the “equation of Niesten”. However, the results from this equation lack a proper validation. We will use our data to validate the results and to determine if the suggested relation exists in four transects around the scour hole (figure 4.4).

$$\frac{p_n}{\rho g} = -\frac{1}{g} \int_{z'}^{h_s} \left(\frac{\partial w}{\partial t} + u \frac{\partial w}{\partial x} + v \frac{\partial w}{\partial y} - \frac{1}{\rho} \left(\frac{\partial \tau_{xz}}{\partial x} + \frac{\partial \tau_{yz}}{\partial y} \right) \right) dz - \frac{w^2}{2g} + \frac{\sigma_{zz}}{\rho g}$$

Niesten assumed that the time derivative, the transverse acceleration, the shear stress gradients and the normal stress may be ignored, because the magnitudes of these terms were two orders smaller than the streamwise flow acceleration and vertical flow velocity in her dataset. Therefore, she could simplify her equation, before using it to obtain the non-hydrostatic pressure head.

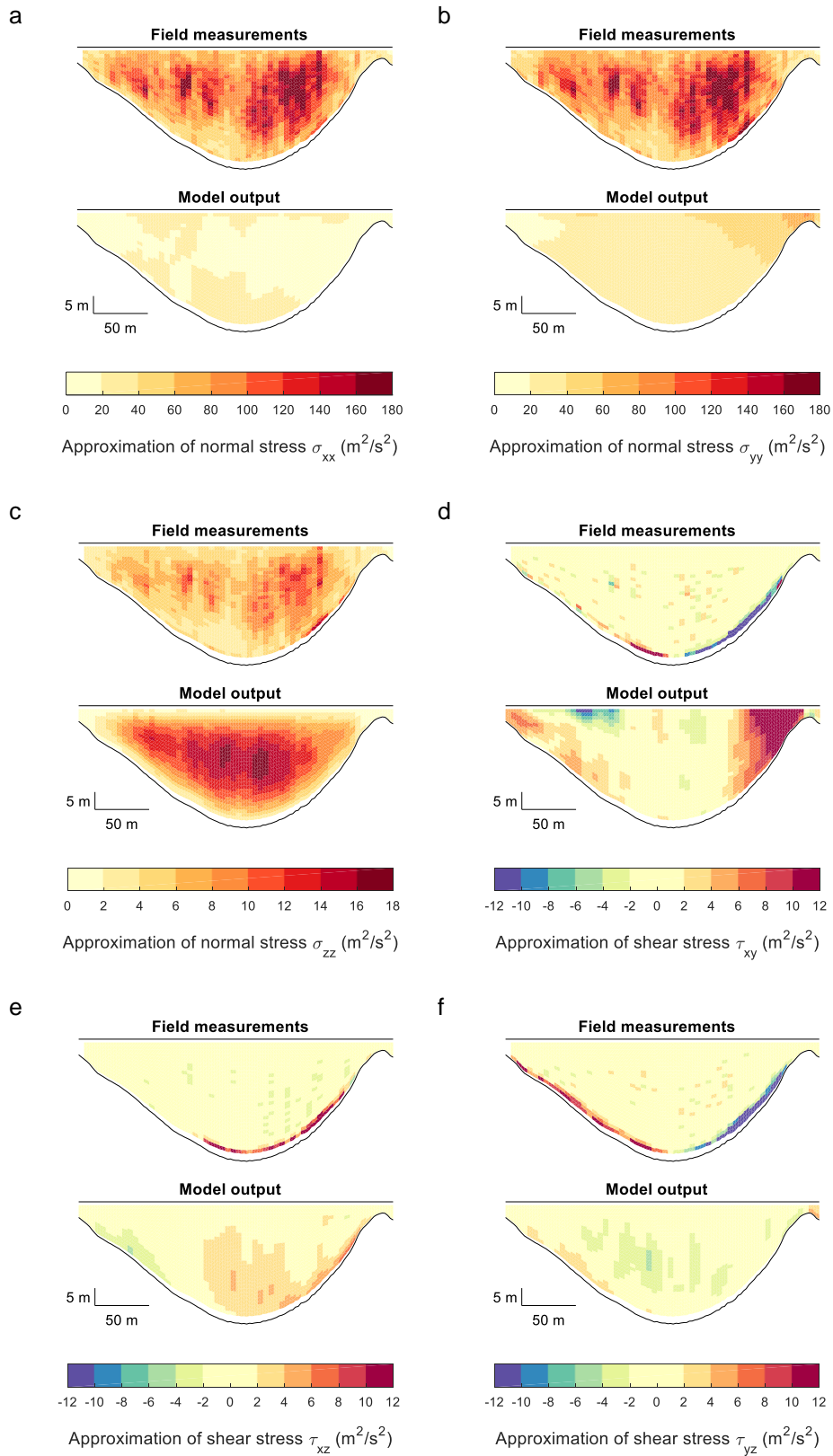


FIGURE 4.3 - APPROXIMATION OF NORMAL (A,B,C) AND SHEAR STRESSES (D,E,F) FROM FIELD MEASUREMENTS AND MODEL OUTPUT

$$\frac{p_n}{\rho g} = -\frac{1}{g} \int_{z'}^{h_s} u \frac{\partial w}{\partial x} dz - \frac{w^2}{2g}$$

First, we apply this simplified equation of Niesten to determine if it is possible to approximate the non-hydrostatic pressure only from flow velocity data. Therefore, we use the field measurements and compare the results with the non-hydrostatic pressure head, as obtained directly from the model output. The approximation of the non-hydrostatic pressure head with the simplified equation of Niesten (figure 4.5a) shows large differences with the direct obtained non-hydrostatic pressure head from the model output (figure 4.5c). Although there are some differences between the flow velocities in the measurements and the model output, they cannot explain this failure (figure 4.5b).

Moreover, the results obtained with the equation of Niesten (figure 4.5a-b) seem to have more in common with each other, than with the direct obtained non-hydrostatic pressure head (figure 4.5c). Therefore, the cause of the failure can probably be attributed to the assumptions which led to the simplification proposed by Niesten. We check these assumption by calculating the order of magnitude of each term in the model output for cross-section 3, because the largest deviations from the hydrostatic pressure head are found at that transect. Because the model was unable to predict the time derivative, we could not take this term into account. However, in the field measurements the time derivative is of an order 10^{-6} , which is much smaller than some other terms, so this term is probably not related to the observed difference.

TABLE 4.1 - ORDERS OF MAGNITUDE OF THE TERMS IN THE EQUATION OF NIESTEN FOR CROSS-SECTION 3

$\frac{1}{g} \int_{z'}^{h_s} u \frac{\partial w}{\partial x} dz$	$\frac{1}{g} \int_{z'}^{h_s} v \frac{\partial w}{\partial y} dz$	$\frac{1}{g} \int_{z'}^{h_s} \frac{1}{\rho} \frac{\partial \tau_{xz}}{\partial x} dz$	$\frac{1}{g} \int_{z'}^{h_s} \frac{1}{\rho} \frac{\partial \tau_{yz}}{\partial y} dz$	$\frac{w^2}{2g}$	$\frac{\sigma_{zz}}{\rho g}$
10^{-4}	10^{-4}	10^{-7}	10^{-7}	10^{-5}	10^{-3}

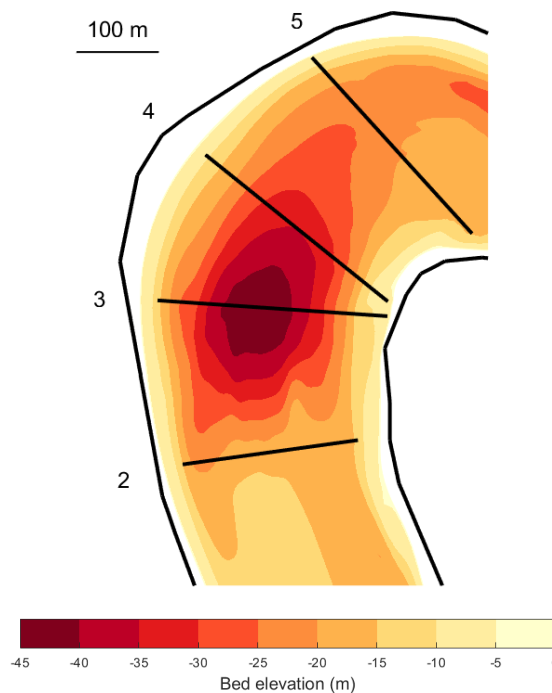


FIGURE 4.4 - TRANSECTS AROUND SCOUR HOLE IN SHARP BEND WHERE WE OBTAINED THE NON-HYDROSTATIC PRESSURE HEAD

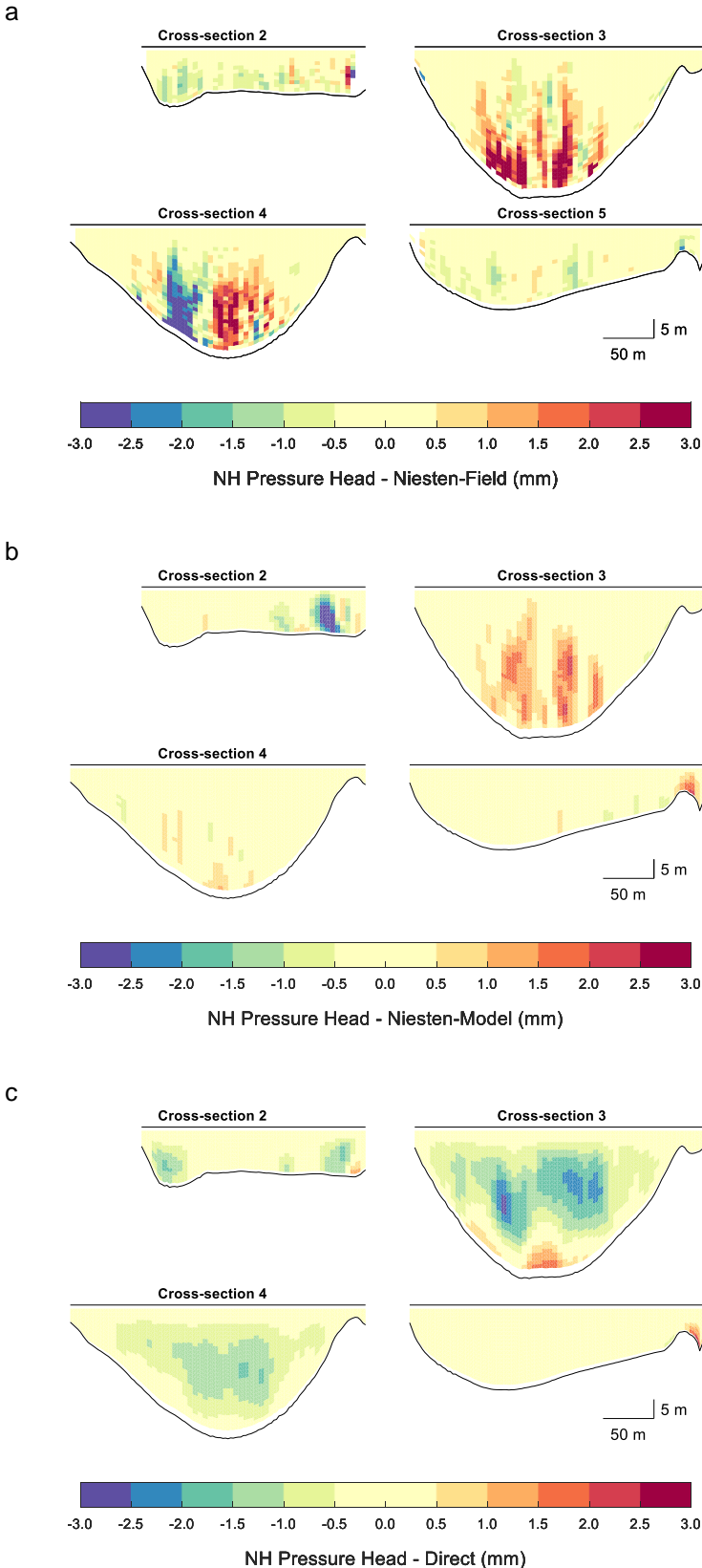


FIGURE 4.5 OBTAINING THE NON-HYDROSTATIC PRESSURE HEAD WITH THE EQUATION OF NIESTEN (A-B) AND DIRECTLY FROM THE MODEL OUTPUT (C)

The orders of magnitude (table 4.1) make clear that the assumptions made by Niesten do not apply for our case. The transverse flow acceleration and the normal stress cannot be ignored, while we can ignore the vertical flow velocity, because it is two orders smaller than the normal stress. So, we can still simplify the equation for the determination of the non-hydrostatic pressure head, but include other terms. We call this the “revised equation”.

$$\frac{p_n}{\rho g} = -\frac{1}{g} \int_{z'}^{h_s} \left(u \frac{\partial w}{\partial x} + v \frac{\partial w}{\partial y} \right) dz + \frac{\sigma_{zz}}{\rho g}$$

The similarity between the results from the revised equation with model output (figure 4.6b) and the direct model output (figure 4.5c), is much larger than between the equation of Niesten with model output (figure 4.5b) and the direct model output. The similarity also increases when the revised equation is used with field measurements (figure 4.6a). However, the difference with the direct obtained non-hydrostatic pressure head, is larger than in the revised equation with model output. This is probably caused by the difference in flow velocities between the field measurements and the model simulations, because the differences between the results from the revised equation (figure 4.6a-b) are the same as when the equation of Niesten was used (figure 4.5a-b). Moreover, instrument noise causes an unreliable prediction of the normal stress in the field measurements.

The non-hydrostatic pressure head from the revised equation shows the same pattern as in the direct model output. The small differences may be caused by calculation errors. So, this evaluation shows that the suggestion of Vermeulen (2015) and Niesten (2016) about the relation between the non-hydrostatic pressure and the vertical flow accelerations is probably wrong, and that we should take the turbulent stresses into account to understand the origin of non-hydrostatic pressure. Therefore, we cannot assume an inviscid flow based on the relation between vertical flow accelerations and non-hydrostatic pressure.

4.3 Hydrodynamic processes

The study about the origin of the non-hydrostatic pressure around the scour hole revealed that we cannot use a relation between vertical flow acceleration and non-hydrostatic pressure to assume inviscid flow. However, this does not mean that we directly have to reject the inviscid flow assumption, we only evaluated a few cross-sections. To determine if this assumption holds, we evaluate the cross-sectional absolute values of the acceleration, pressure gradient and turbulent stress gradient in the streamwise (figure 4.8a), transverse (figure 4.8b) and vertical (figure 4.8c) momentum balance for the 800 interpolated transects along the scour hole (figure 4.7).

In the appendices, we show that the presented patterns are not largely influenced by taking the cross-sectional average (appendix A) and using the average acceleration and turbulent stress gradient (appendix B).

<i>Acceleration</i>	<i>Pressure gradient</i>	<i>Turbulent stress gradient</i>
$\left u \frac{\partial u}{\partial x} + v \frac{\partial u}{\partial y} + w \frac{\partial u}{\partial z} \right $	$= \left -\frac{1}{\rho} \frac{\partial p}{\partial x} \right $	$+ \left \frac{1}{\rho} \left(\frac{\partial \sigma_{xx}}{\partial x} + \frac{\partial \tau_{yx}}{\partial y} + \frac{\partial \tau_{zx}}{\partial z} \right) \right $
$\left u \frac{\partial v}{\partial x} + v \frac{\partial v}{\partial y} + w \frac{\partial v}{\partial z} \right $	$= \left -\frac{1}{\rho} \frac{\partial p}{\partial y} \right $	$+ \left \frac{1}{\rho} \left(\frac{\partial \tau_{xy}}{\partial x} + \frac{\partial \sigma_{yy}}{\partial y} + \frac{\partial \tau_{zy}}{\partial z} \right) \right $
$\left u \frac{\partial w}{\partial x} + v \frac{\partial w}{\partial y} + w \frac{\partial w}{\partial z} \right $	$= \left -\frac{1}{\rho} \frac{\partial p_n}{\partial z} \right $	$+ \left \frac{1}{\rho} \left(\frac{\partial \tau_{xz}}{\partial x} + \frac{\partial \tau_{yz}}{\partial y} + \frac{\partial \sigma_{zz}}{\partial z} \right) \right $

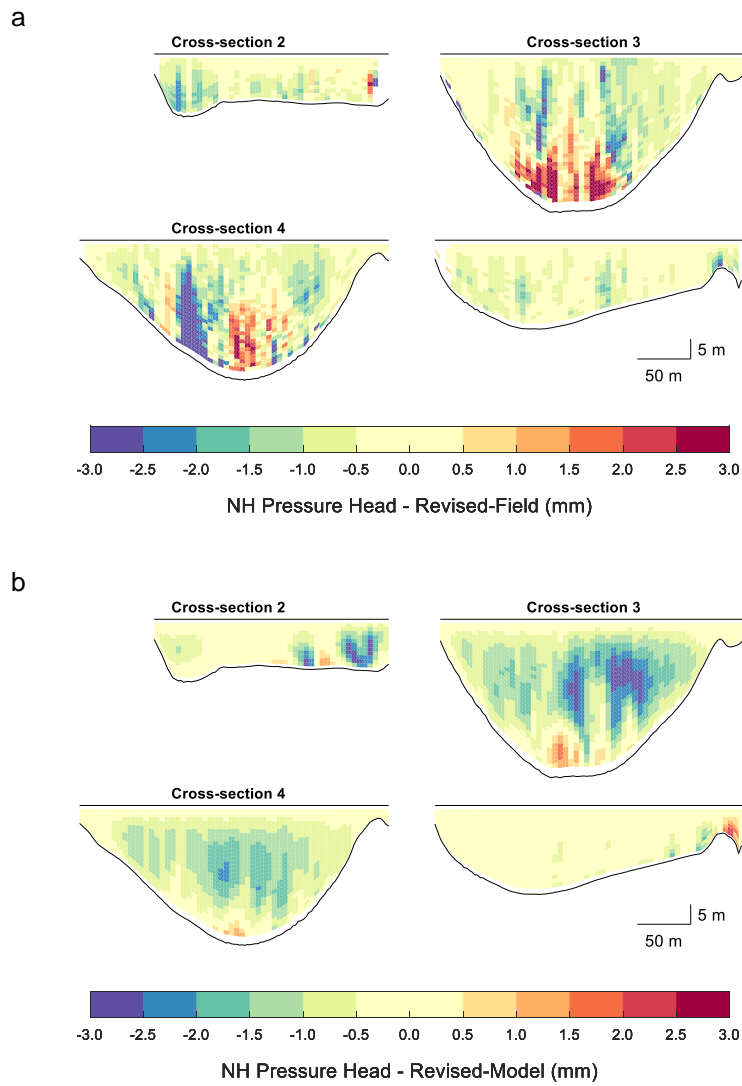


FIGURE 4.6 – NON-HYDROSTATIC PRESSURE HEAD OBTAINED WITH THE REVISED EQUATION FROM FIELD MEASUREMENTS (A) AND MODEL OUTPUT (B)

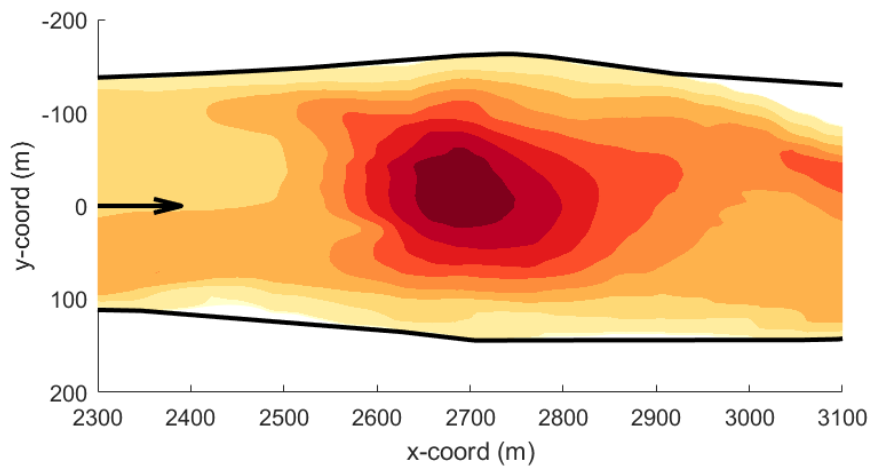


FIGURE 4.7 - COORDINATES OF TRANSFORMED MODEL OUTPUT

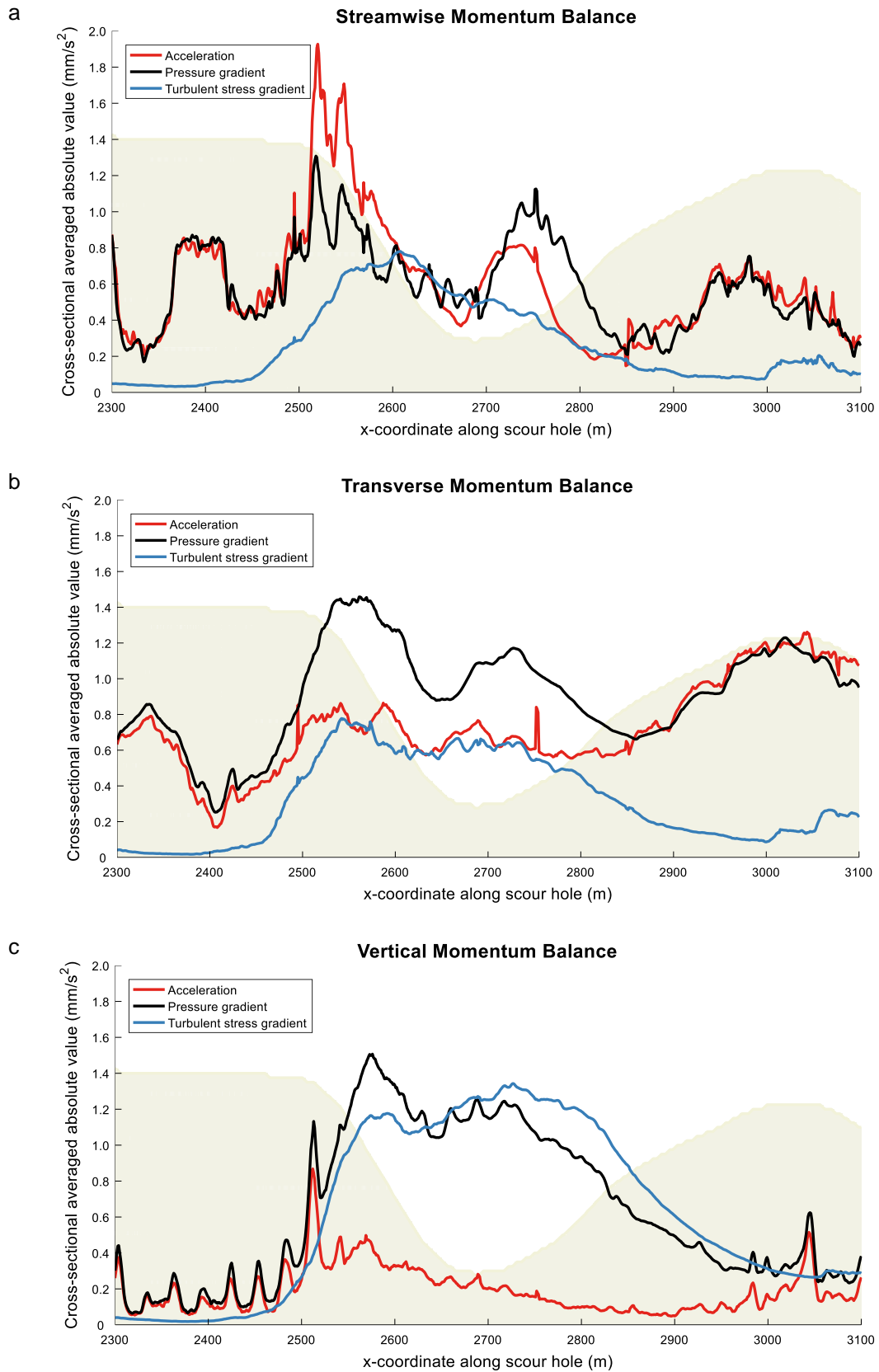


FIGURE 4.8 –HYDRODYNAMIC PROCESSES ALONG SCOUR HOLE IN STREAMWISE (A), TRANSVERSE (B) AND VERTICAL (C) MOMENTUM BALANCE

In each of the three patterns (figure 4.8), we see that the momentum balances upstream and downstream of the scour hole are dominated by acceleration and the pressure gradient. So, in these river sections, we may assume an inviscid flow. Around the scour hole, however, the turbulent stress gradient increases. In the streamwise and transverse balance, the turbulent stress gradient and the acceleration show about the same values around the deepest part of the scour hole. In the vertical balance, the turbulent stress gradient becomes more than 6 times larger than the acceleration. The pressure gradient shows also a large increase in that area. Therefore, we may conclude that the inviscid flow assumption is not valid in the scour hole.

Particularly in the streamwise and transverse balance, the increase of the turbulent stress gradient is limited to the location of the scour hole (figure 4.8a-b). Upstream of the scour hole, the river shows a straight topography, in which an inviscid flow can often be assumed (Fox, et al., 2011). However, downstream of the scour hole, we find the sharp bend. Although the curvature related forces initiate a secondary flow, flow separation and superelevation, these processes seem not to increase the turbulence.

The large peak of acceleration at the entrance of the scour hole in the streamwise momentum balance (figure 4.8a), may be explained from the decreased average flow and flow separation in this area (figure 4.9). The increase in cross-sectional area at the entrance of the scour hole reduces the average flow velocity, so the flow will decelerate. Moreover, the flow separates near the banks, which will cause the deceleration to become even larger. The absolute value of these decelerations is probably causing the large peak at the entrance of the scour hole.

The peaks in the pressure gradient in the streamwise balance at the entrance and exit of the scour hole (figure 4.8a), are probably caused by the increased water surface elevation due to the increased cross-sectional area (figure 2.6b). The hydrostatic part of the pressure gradient in streamwise direction originates from the modelled water surface elevation. So, our understanding of the changing surface elevation above the scour hole may explain the peaks in the pressure gradient. The largest water surface level is found above the deepest part of the scour hole, so the largest pressure gradients must be found just upstream and downstream of this location.

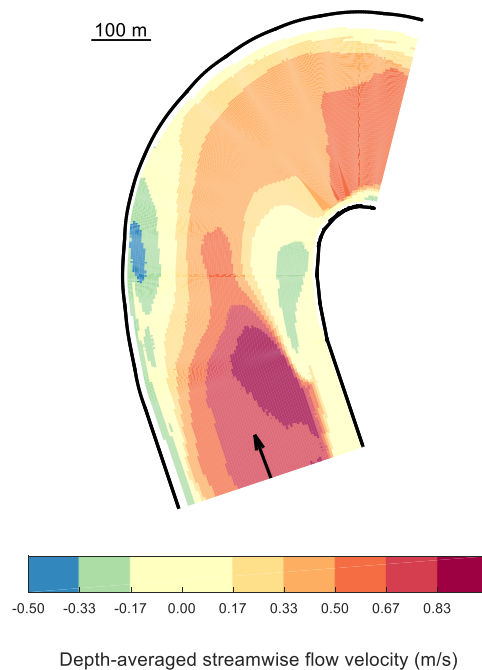


FIGURE 4.9 - DEPTH-AVERAGED STREAMWISE FLOW VELOCITY ALONG THE SHARP BEND

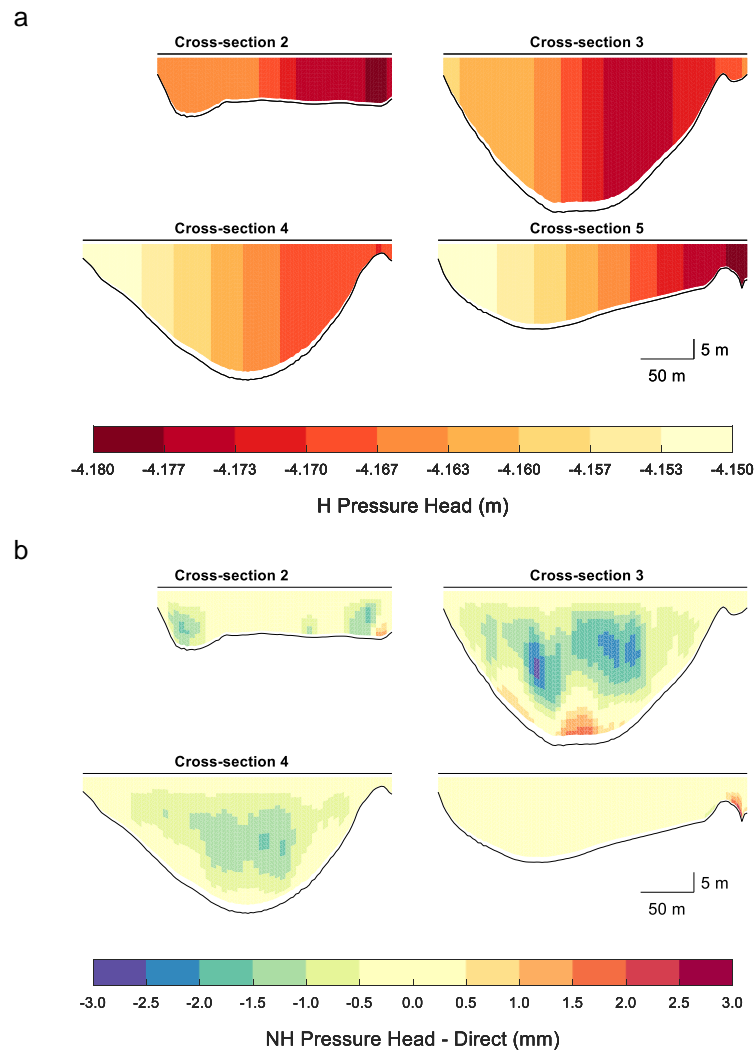


FIGURE 4.10 - HYDROSTATIC (A) AND NON-HYDROSTATIC (B) PRESSURE HEAD FROM THE MODEL SIMULATIONS

In the transverse momentum balance (figure 4.8b), the large values of the pressure gradient can also be explained from the water surface level. However, in this balance, the gradient originates not from the increased cross-sectional area, but from the superelevation in the sharp bend (figure 2.6a). The superelevation increases the water level in the outer bend, and decreases it in the inner bend. Therefore, a gradient in transverse direction can be found. This also explains why the pressure gradient remains large, and even increases, downstream of the scour hole, because the point of highest curvature is located downstream of the scour hole.

The pressure gradient in the vertical momentum balance is completely non-hydrostatic, because the hydrostatic part equals the gravity acceleration. Because this term is remarkably large, it is interesting to determine how the non-hydrostatic part of the pressure gradient in the other two balances behaves. The difference between the hydrostatic pressure head and non-hydrostatic pressure head, is about 3 orders of magnitude. However, difference between the range over which the pressure varies within a cross-section, is only a factor 5 (figure 4.10).

Therefore, the non-hydrostatic pressure gradient may also have a significant contribution in the streamwise and transverse momentum balance. This suggestion is supported by the streamwise momentum balance, in which the total pressure gradient is divided into a hydrostatic pressure gradient and a non-hydrostatic pressure gradient (figure 4.11a). The largest deviations of the non-

hydrostatic pressure are found around the entrance of the scour hole, where it in some transects even exceeds the hydrostatic pressure gradient. We note here that we did not use the absolute values in this evaluation, because the balance between the three pressure gradients is not visible in that case.

$$\frac{1}{\rho} \frac{\partial p}{\partial x} - \frac{1}{\rho} \frac{\partial p_h}{\partial x} - \frac{1}{\rho} \frac{\partial p_n}{\partial x} = 0$$

In the transverse momentum balance (figure 4.11b), however, a significant non-hydrostatic pressure gradient is not visible. The non-hydrostatic pressure gradient in this balance remains between 5 and 10 times smaller than the hydrostatic pressure gradient. Therefore, it seems that the non-hydrostatic pressure is quite constant over width and not related to curvature. The same patterns are also found locally and seem not to be influenced by taking the cross-sectional average value (appendix A).

$$\frac{1}{\rho} \frac{\partial p}{\partial y} - \frac{1}{\rho} \frac{\partial p_h}{\partial y} - \frac{1}{\rho} \frac{\partial p_n}{\partial y} = 0$$

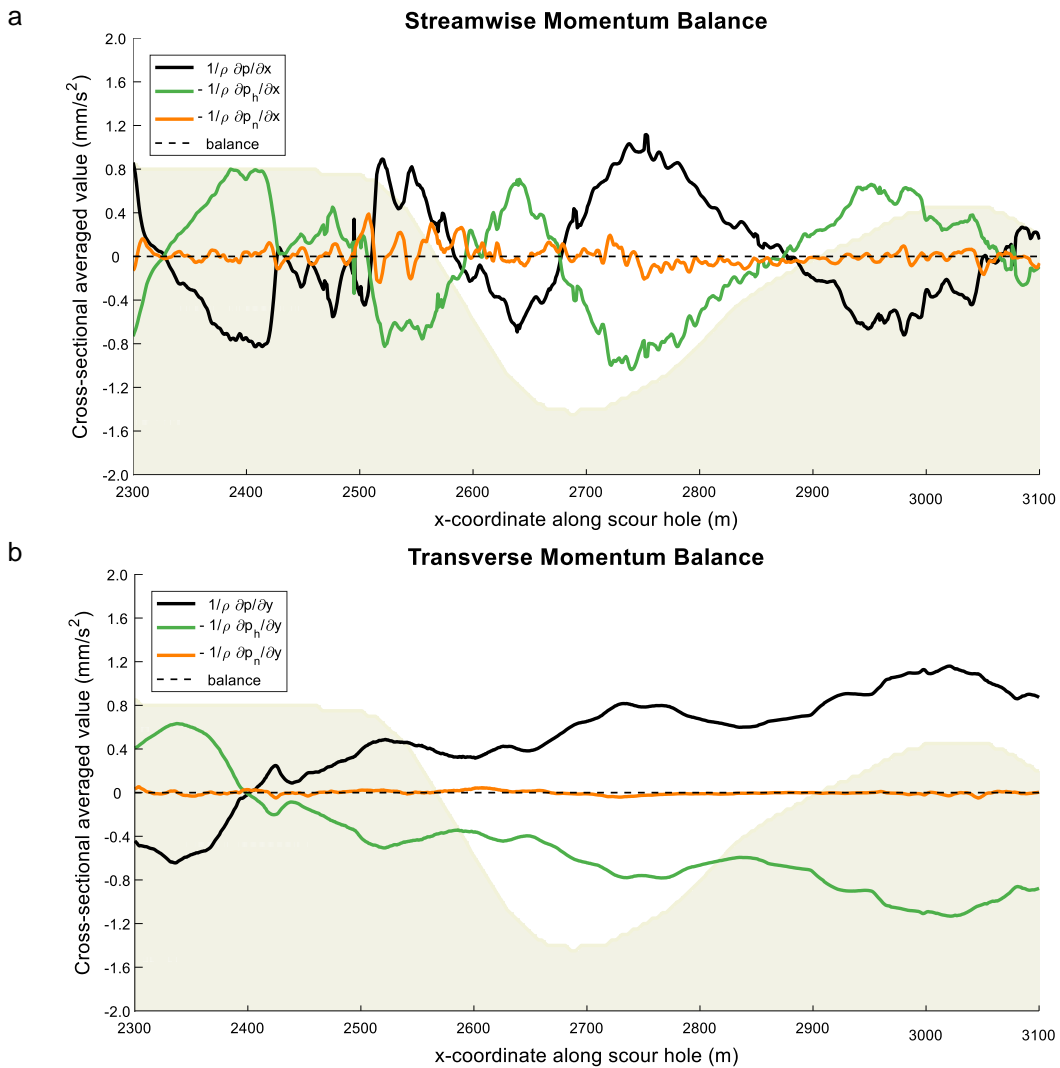


FIGURE 4.11 - HYDROSTATIC AND NON-HYDROSTATIC PRESSURE GRADIENT IN STREAMWISE (A) AND TRANSVERSE (B) MOMENTUM BALANCE

4.4 Vertical momentum balance

We could explain most of the observed patterns in the streamwise and transverse momentum balance from our current understanding of scour holes in sharp bends. However, in the vertical momentum balance, we observe a huge increase of the pressure gradient and the turbulent stress gradient, particularly when we compare these terms with the acceleration. Previous studies did comment on the role of turbulent stresses around scour holes, but they also assumed the accelerations to be important. In our result, the balance is dominated by the pressure gradient and the turbulent stress gradient, and the acceleration is much smaller. Because such large deviation from the inviscid flow assumption seems to be important to understand scour hole processes, we will study the hydrodynamic processes of the vertical balance in detail.

$$u \frac{\partial w}{\partial x} + v \frac{\partial w}{\partial y} + w \frac{\partial w}{\partial z} = -\frac{1}{\rho} \frac{\partial p_n}{\partial z} + \frac{1}{\rho} \left(\frac{\partial \tau_{xz}}{\partial x} + \frac{\partial \tau_{yz}}{\partial y} + \frac{\partial \sigma_{zz}}{\partial z} \right)$$

We already used the vertical momentum balance to validate the equation of Niesten. In the application of this equation, we observed a large contribution of the normal stress in the generation of the non-hydrostatic pressure head (table 4.1). If we observe the balance in which each term is included, we see also that the gradient of the normal stress is large (figure 4.12). Together with the non-hydrostatic pressure gradient, they dominate the balance above the scour hole. Only upstream and downstream of the scour hole, the normal stress gradient is not a dominant factor. In these parts, the streamwise acceleration balances the pressure gradient.

To get more insight in the cause of the large changes around the scour hole, we evaluate the distribution of the dominant terms in the balance at five specific cross-sections (figure 4.12) around the scour hole. The cross-sections are chosen in such way that we can compare the distributions upstream, along and downstream of the scour hole. If we neglect the terms which show no dominance around the scour hole, and put all the terms at the left-hand side of the balance, we get a balance with the streamwise acceleration, non-hydrostatic pressure gradient and normal stress gradient.

$$u \frac{\partial w}{\partial x} + \frac{1}{\rho} \frac{\partial p_n}{\partial z} - \frac{1}{\rho} \frac{\partial \sigma_{zz}}{\partial z} = 0$$

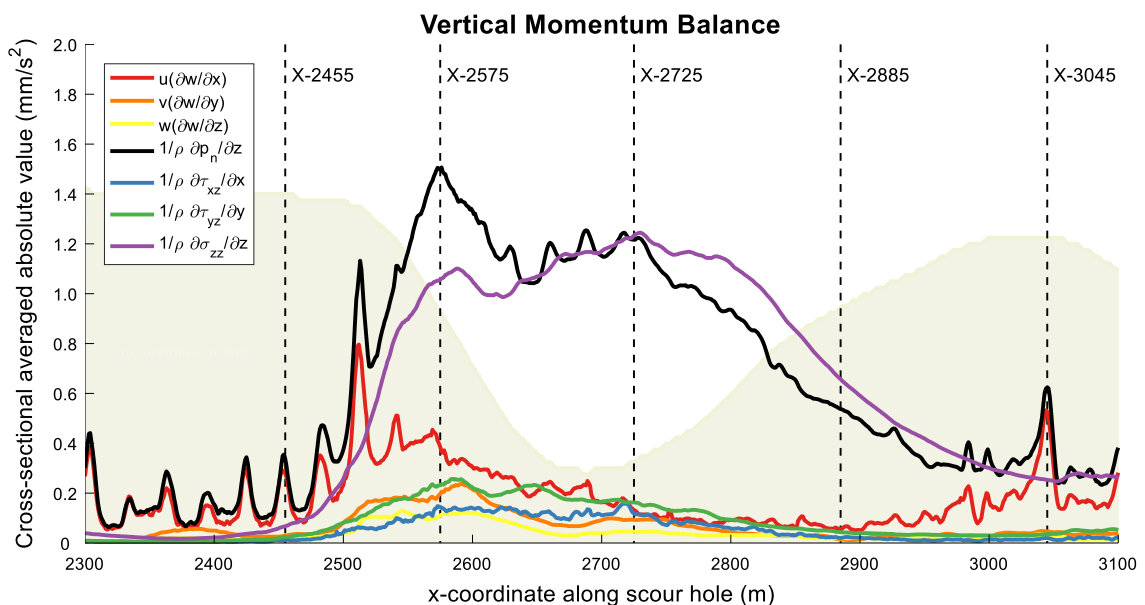


FIGURE 4.12 – CROSS-SECTIONAL AVERAGED ABSOLUTE VALUES OF THE TERMS IN THE VERTICAL MOMENTUM BALANCE

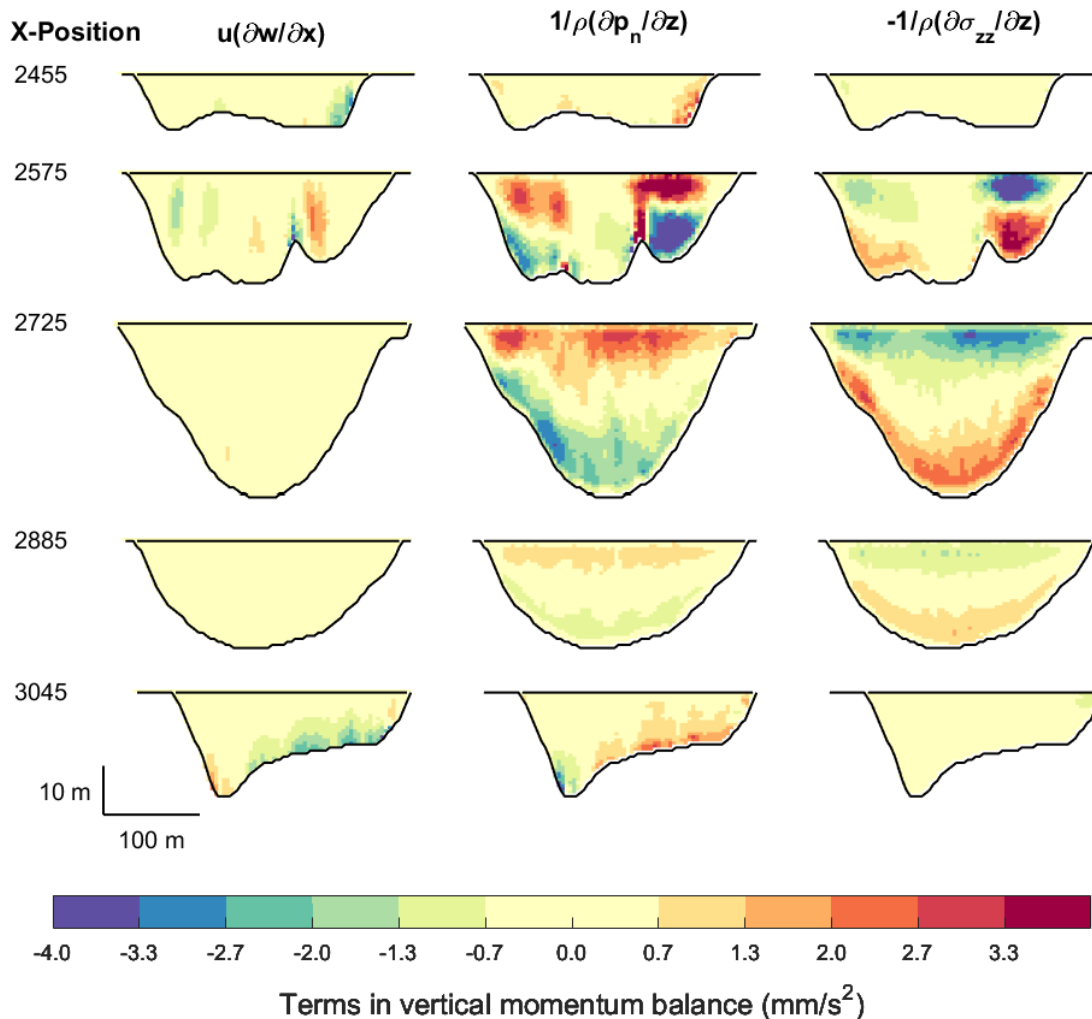


FIGURE 4.13 - CROSS-SECTIONAL VARIATION OF DOMINANT TERMS IN THE VERTICAL MOMENTUM BALANCE

As expected from the cross-sectional averaged terms (figure 4.12), the dominant terms along the scour hole are the pressure gradient and the normal stress gradient (figure 4.13). In the cross-sections within the scour hole, the values are also larger than in the cross-sections upstream and downstream of the scour hole. From the first and last cross-section, we see that the pressure gradient is mainly balanced by the streamwise acceleration. When the pressure gradient increases around the scour hole, the normal stress gradient becomes important. The distributions make quite clear that they balance each other, not only in average, but also locally.

The values of the pressure gradient and normal stress gradient are different of sign between the upper and lower part of the cross-section, and show both a zero region around mid-depth (figure 4.13). For the non-hydrostatic pressure gradient, this pattern can be explained from the fact that the pressure is always hydrostatic at the water surface. Therefore, the non-hydrostatic pressure and its vertical gradient are zero at the water surface level. The largest deviations from hydrostatic pressure are found around mid-depth, and these values are small again near the river bed (figure 4.14). The deviations are negative, because the actual pressure is larger than the hydrostatic pressure. So, this pattern requires large gradients close to the water surface and river bed, which are clearly visible from the distributions (figure 4.13).

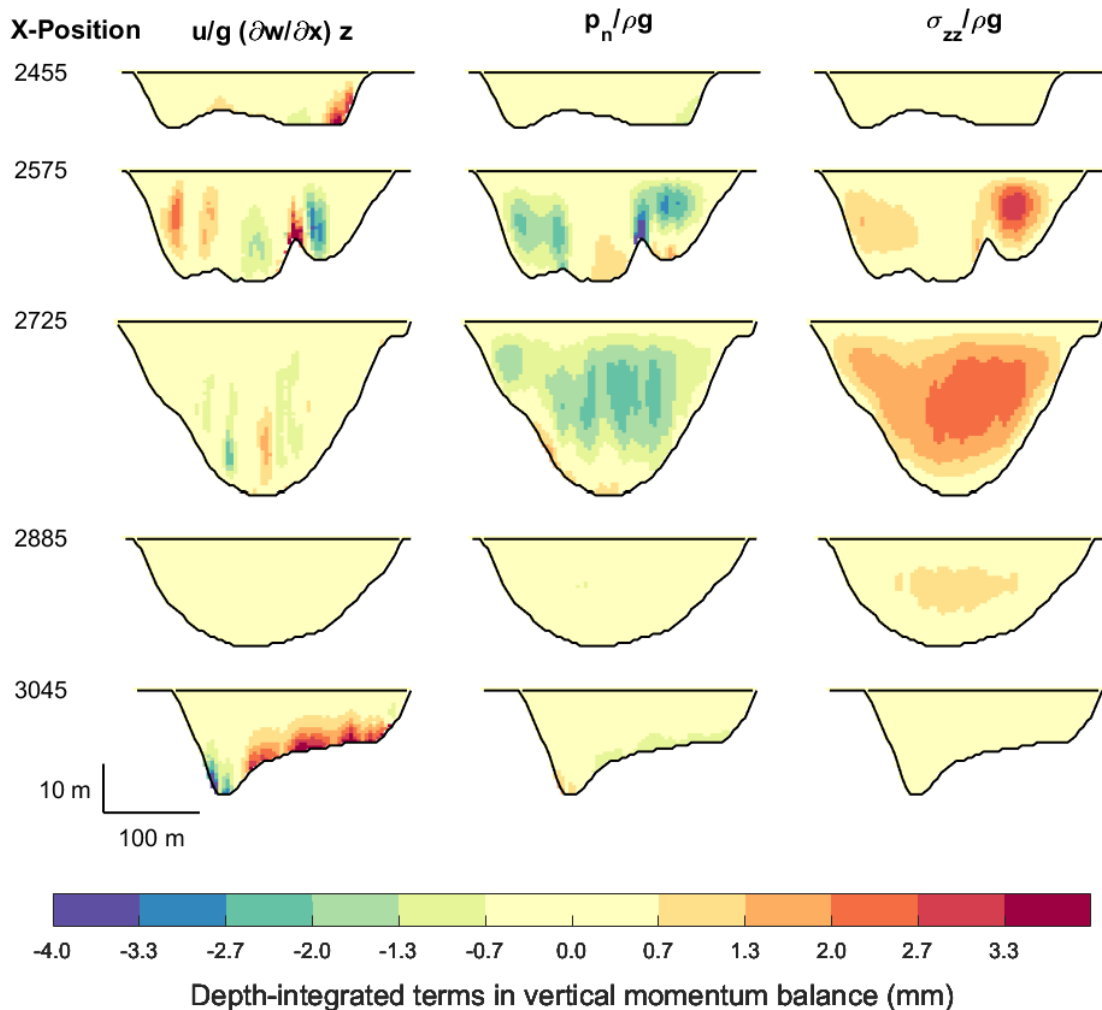


FIGURE 4.14 - CROSS-SECTIONAL VARIATION OF DEPTH-INTEGRATED DOMINANT TERMS IN THE VERTICAL MOMENTUM BALANCE

The vertical gradient of the normal stress has the same pattern, but with opposite sign. This turbulent term is determined from the variance in vertical velocity. Because there is no flow in vertical direction at the water surface and river bed, the vertical velocity is always zero there and so is its variance (Blanckaert & Graf, 2001). The largest variances are found around mid-depth (figure 4.14). Just as with the vertical pressure gradient, the increase from zero at the boundaries to maximum around mid-depth results in the largest gradients in the upper and lower part of the cross-section.

As the vertical component of the normal stress seems to be the most important factor to explain non-hydrostatic pressure around scour holes, we also evaluate its development along the scour hole (figure 4.15). The largest values can be found around mid-depth in the deepest part of the scour hole. The increase in variance around the scour hole may be explained from the larger distance to fixed boundaries. The vertical velocity is restricted to zero at the water surface and the river bed. If the distance between those boundaries is relatively small, they have a large impact on the velocity distribution, which makes fluctuations smaller. In the scour hole, the fixed boundaries are further away, so their impact is smaller, which may result in larger fluctuations and a larger normal stress component.

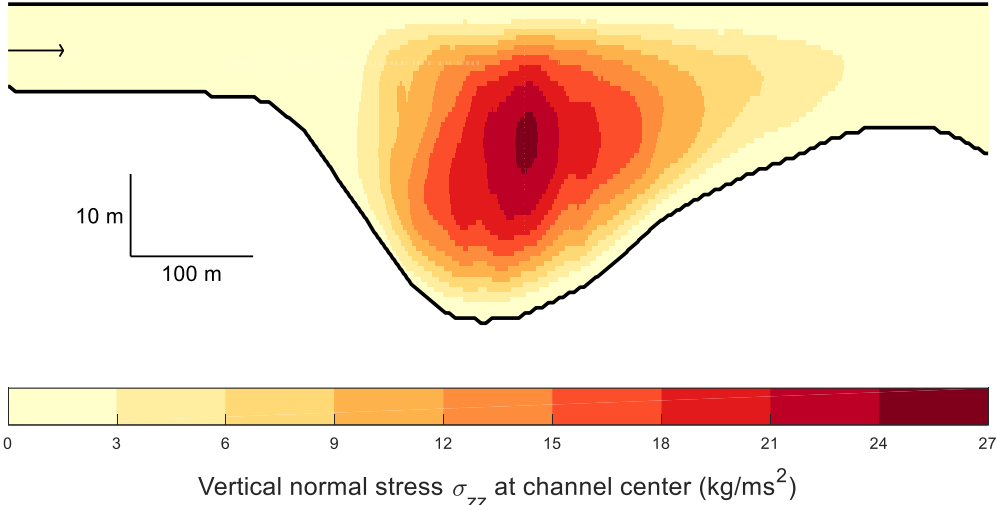


FIGURE 4.15 - VERTICAL NORMAL STRESS ALONG AT THE CHANNEL CENTER OF THE SCOUR HOLE

5 DISCUSSION

In the fifth chapter, we discuss the reliability, limitations and physical meaning of our results. First, we discuss how the choices made in the processing of the data and the differences between the field measurements and the model output may have influenced our results. Thereafter, we continue with a discussion of the physical meaning of our most important results.

5.1 Data processing

In the processing of the field measurements and the model output, we made some choices which may have influenced our results. First, we used the direction of the transects to define our flow directions in the field measurements (figure 5.1a). However, the definitions could also be based on the cross-sectional averaged flow direction (figure 5.1b). The definition of the flow directions is important for obtaining the results. The streamwise and transverse flow velocities in transect 3 show some differences between the two ways of defining the flow directions (figure 5.2). The vertical flow velocity does not change, because the rotation only influences the streamwise and transverse flow direction.

In obtaining the non-hydrostatic pressure head with the equation of Niesten, we used the orders of magnitude of each term to simplify the equation. The way of rotating the flow velocities will change the values in the equation. However, the changes are not large enough to result in another order of magnitude (table 5.1). So, the simplification is the same in both rotations. Therefore, we may conclude that the choice of rotation is not large enough to influence our results.

TABLE 5.1 – CROSS-SECTIONAL AVERAGED ABSOLUTE VALUES OF THE TERMS IN THE EQUATION OF NIESTEN FOR CROSS-SECTION 3

	$\frac{1}{g} \int_{z'}^{h_s} u \frac{\partial w}{\partial x} dz$	$\frac{1}{g} \int_{z'}^{h_s} v \frac{\partial w}{\partial y} dz$	$\frac{1}{g} \int_{z'}^{h_s} \frac{1}{\rho} \frac{\partial \tau_{xz}}{\partial x} dz$	$\frac{1}{g} \int_{z'}^{h_s} \frac{1}{\rho} \frac{\partial \tau_{yz}}{\partial y} dz$
Rotation a	$4.3 * 10^{-4}$	$1.9 * 10^{-4}$	$2.1 * 10^{-7}$	$3.5 * 10^{-7}$
Rotation b	$4.3 * 10^{-4}$	$2.5 * 10^{-4}$	$2.1 * 10^{-7}$	$3.6 * 10^{-7}$

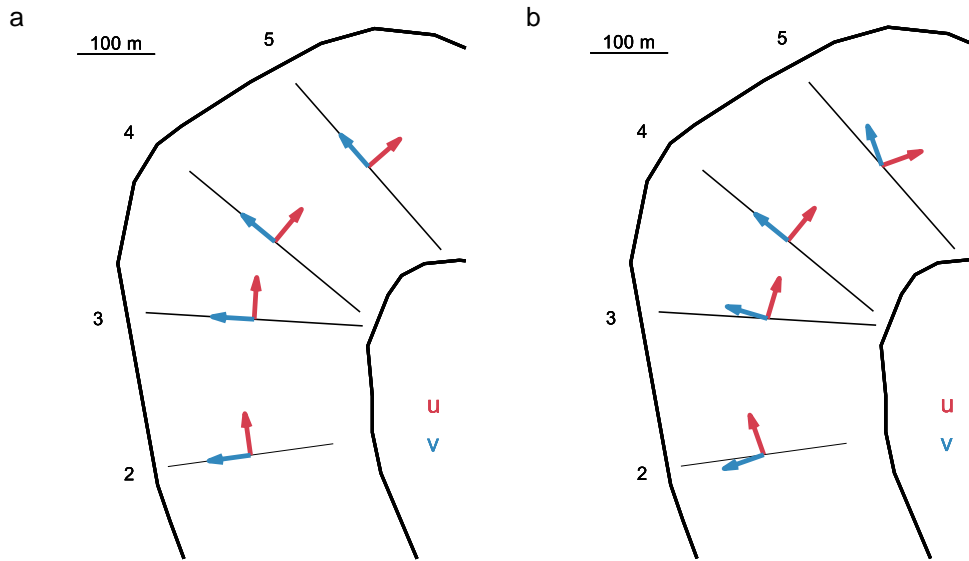


FIGURE 5.1 - ROTATION OF FLOW VELOCITIES TO DIRECTION OF TRANSECTS (A) OR THE CROSS-SECTIONAL AVERAGED FLOW DIRECTION (B)

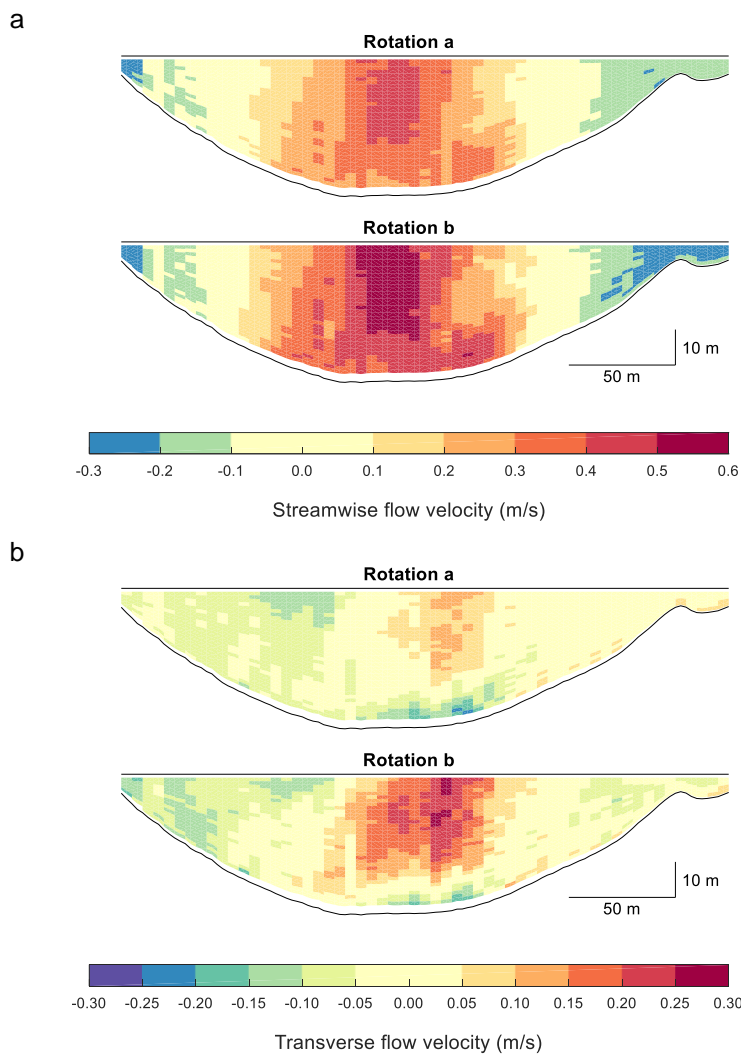


FIGURE 5.2 - STREAMWISE AND TRANSVERSE FLOW VELOCITY FROM DIFFERENT ROTATIONS IN TRANSECT 3

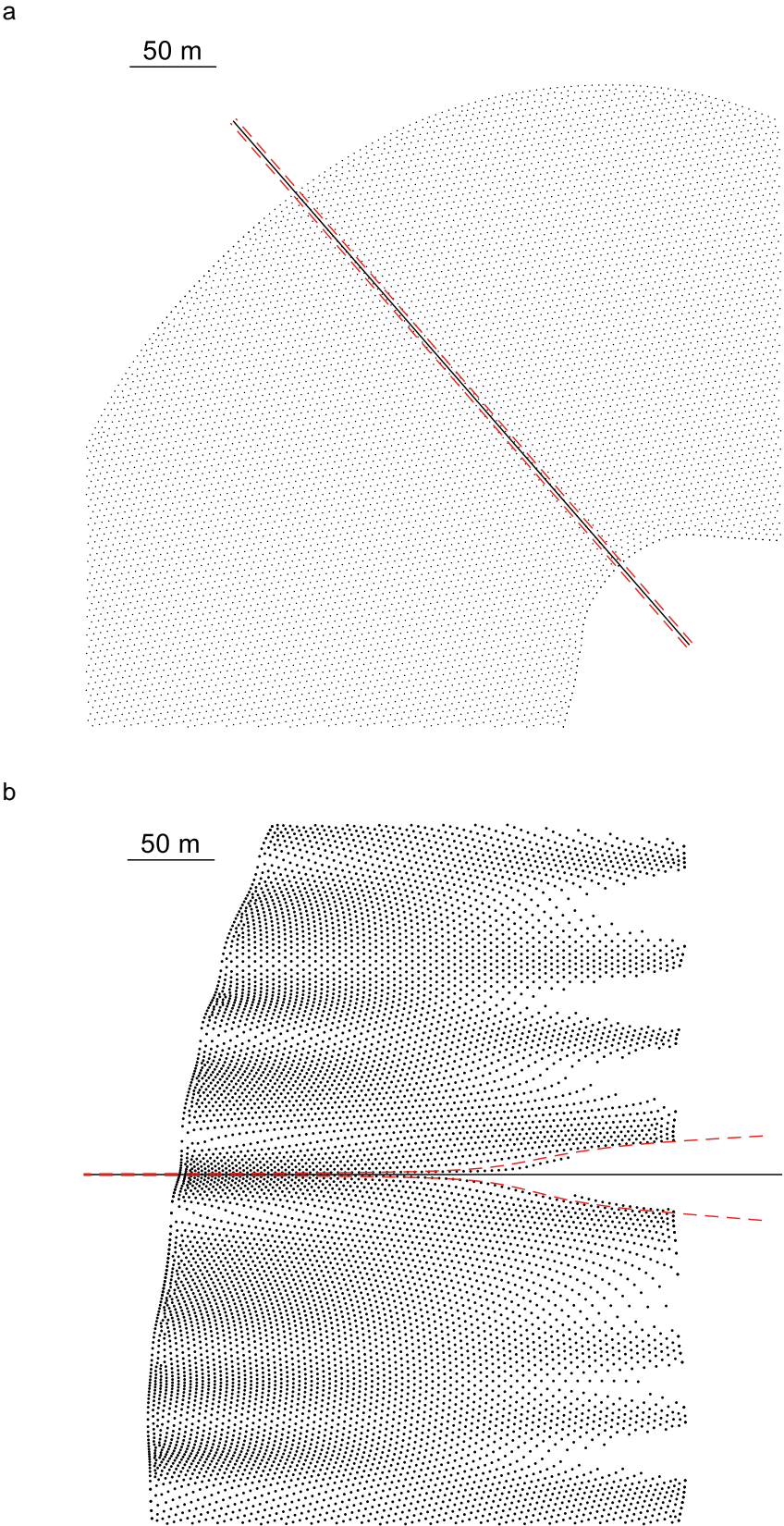


FIGURE 5.3 – CALCULATING THE GRADIENT OVER X-DIRECTION IN FROM THE ORIGINAL (A) AND TRANSFORMED (B) MODEL OUTPUT

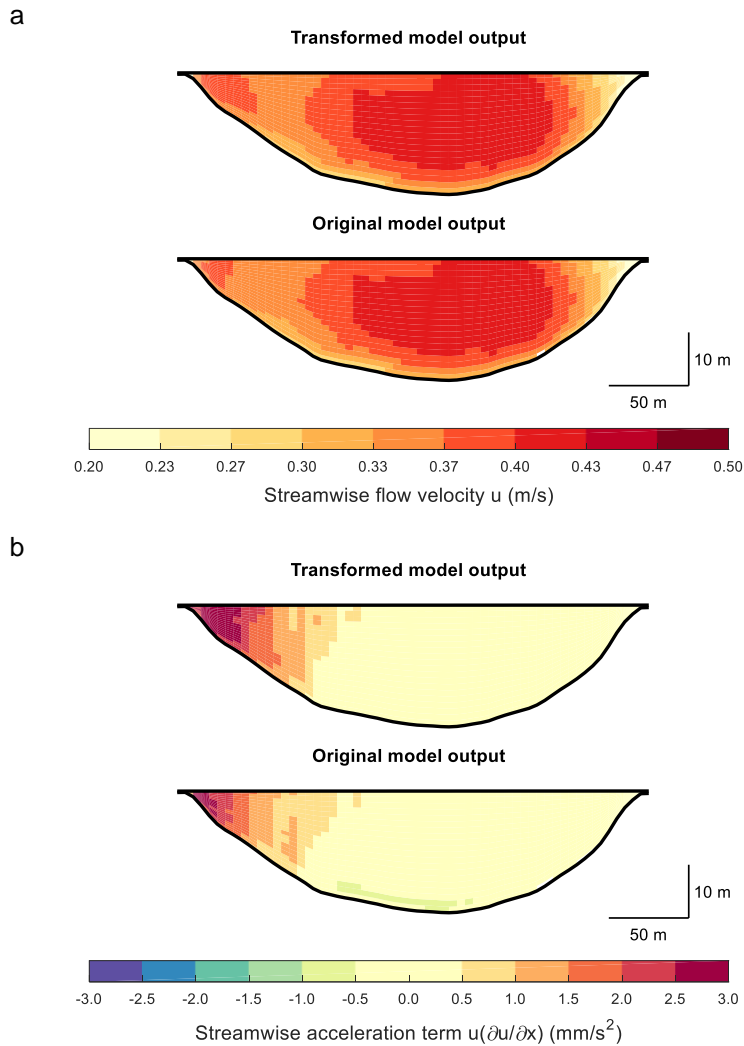


FIGURE 5.4 - STREAMWISE VELOCITY (A) AND ITS ACCELERATION OVER X (B) IN TRANSFORMED AND ORIGINAL MODEL OUTPUT

The comparison of the two ways of rotation is limited to the coordinate system of the original model output. However, most of the results were obtained from the interpolation to the transects in the transformed model output. In the transformation, we changed the curved river center line into a straight line. The resulting constant coordinate system made it easier to evaluate the hydrodynamic processes. However, the transformation may have influenced our results.

The data points in the original model output are equally spread over the whole bend (figure 5.3a). So, an interpolation to a single transect is always based on the same amount of surrounding data points. After the transformation, the data points in the outer bend are located closer to each other, while the data points in the inner bend show larger distances (figure 5.3b). Therefore, the interpolation from the transformed model output to a single transect, may be based from a different number of data points in the inner and outer bend. Moreover, the larger distances between the data points in the inner bend, may smooth the results. Therefore, the approximation of the results from the transformed dataset may be a bit unreliable.

To determine if the results after the transformation differ from the original model output, we compare the streamwise flow velocity and its acceleration term in x -direction, in a transect from the original model output (figure 5.3a) with the same transect in the transformed model output (figure 5.3b). In the inner bend of the transformed transect, no data points close to the transect are

visible. So, the data is interpolated to this transect from a larger distance than in the transect from the original model output. In the case of the gradient over x -direction, a constant dx in the original model output, results in a changing dx in the transformed data (figure 5.3b). However, in the calculation of du/dx from the transformed output, we use the same constant dx as in the original output, to prevent an error from the transformation.

The resulting values in these transects (figure 5.4) show for both the streamwise velocity and its acceleration over x -direction only small differences. The cross-sectional averaged absolute value of the streamwise velocity increases in the transformed model output from 0.34 m/s to 0.35 m/s. The acceleration term in x -direction decreases in the transformed model output from 2.4 mm/s² to 1.6 mm/s². Although this can be explained as a decrease by a factor 2/3, the difference in value is only 0.8 mm/s², so the influence on the results will be small. Therefore, we may conclude that the transformation of our dataset has probably not caused large errors in the values which were used to evaluate the hydrodynamic processes.

5.2 Model reliability

The way of rotating and transforming the model output, seems not to have a significant impact on the values used to obtain our results. However, this sensitivity analysis does not reveal anything about the reliability of the model itself, only about the influence of different ways in using that data. In the results, we showed the main differences between the field measurements and the model output. The model simulations underestimate the plunging pattern of the flow, and overestimate the turbulent stresses. If the model output consists of exact the same values as in the field measurements, our results may have been different.

We used the model output to determine the orders of magnitude of the terms in the equation of Niesten, and based our simplification on these results. However, the values of the terms are probably different, when they are obtained from the field measurements. If these differences are larger than an order of magnitude, they may result in another conclusion about whether a term should or should not be included in the revised equation of Niesten. The comparison of the values (table 5.2) shows that the value of the normal stress term in the field measurements is half of the value in the model simulations. Therefore, the order of magnitude decreases from 10^{-3} to 10^{-4} .

The values of the flow accelerations and the vertical flow velocity are larger in the field, but do not change from order. However, because the normal stress decreased with one order, the vertical velocity term should be included in the equation, as it is within an order of the largest term. The shear stress gradients are also in the field measurements much smaller than the other terms. So, based on these differences, we propose to include the vertical velocity term in the equation.

$$\frac{p_n}{\rho g} = -\frac{1}{g} \int_{z'}^{h_s} \left(u \frac{\partial w}{\partial x} + v \frac{\partial w}{\partial y} \right) dz - \frac{w^2}{2g} + \frac{\sigma_{zz}}{\rho g}$$

TABLE 5.2 – CROSS-SECTIONAL AVERAGED ABSOLUTE VALUES OF THE TERMS IN THE EQUATION OF NIESTEN FOR CROSS-SECTION 3

	$\frac{1}{g} \int_{z'}^{h_s} u \frac{\partial w}{\partial x} dz$	$\frac{1}{g} \int_{z'}^{h_s} v \frac{\partial w}{\partial y} dz$	$\frac{w^2}{2g}$	$\frac{1}{g} \int_{z'}^{h_s} \frac{1}{\rho} \frac{\partial \tau_{xz}}{\partial x} dz$	$\frac{1}{g} \int_{z'}^{h_s} \frac{1}{\rho} \frac{\partial \tau_{yz}}{\partial y} dz$	$\frac{\sigma_{zz}}{\rho g}$
Field	$6.5 * 10^{-4}$	$2.7 * 10^{-4}$	$9.3 * 10^{-5}$	$0.7 * 10^{-7}$	$3.3 * 10^{-7}$	$7.0 * 10^{-4}$
Model	$4.3 * 10^{-4}$	$1.9 * 10^{-4}$	$3.1 * 10^{-5}$	$2.1 * 10^{-7}$	$3.5 * 10^{-7}$	$1.4 * 10^{-3}$

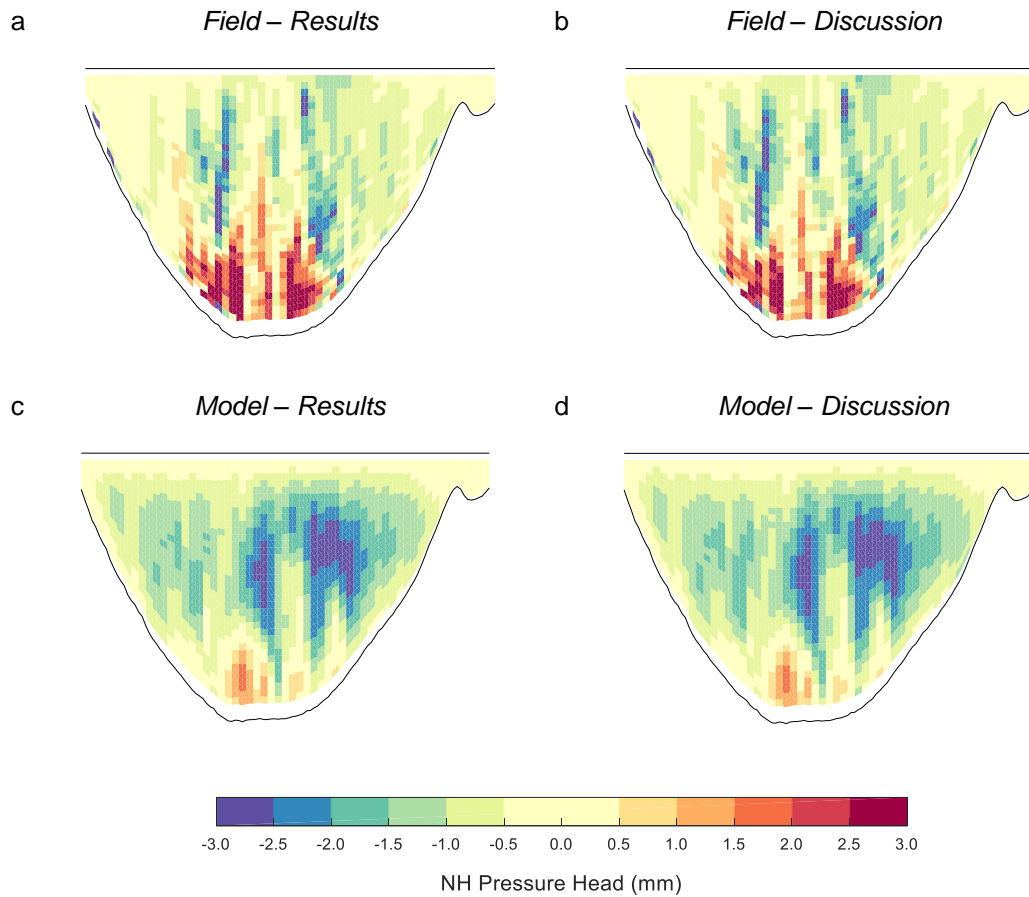


FIGURE 5.5 - NON-HYDROSTATIC PRESSURE HEAD FROM FIELD MEASUREMENTS AND MODEL OUTPUT WITH EQUATION PRESENTED IN RESULTS (A-C) AND DISCUSSION (B-D) FOR CROSS-SECTION 3

However, for both field measurements (figure 5.5a-b) and the model output (figure 5.5c-d), changing the equation does only result in small changes. Particularly, when we compare this difference with the difference between the field measurements and the model output. The data used as input in the equation has a much larger effect on the result, than whether the vertical velocity is included in the equation. So, we may conclude that the difference between the field measurements and the model output is indeed influencing our results, however, not due to a change in the used equation.

To determine how the differences between the field measurements and the model output may have influenced the rest of our results, we use the differences to modify these results. From the differences in magnitude between both datasets, we calculate a modification factor (table 5.3). This factor is an indicator of the error in the model simulation for a single term. As the area around the scour hole is most important for our study, we base the modification factor mainly on the differences in cross-section 3 and 4.

The terms in the RANS equations were multiplied by the modification factors. Thereafter, we determined the same balances as in the results (figure 5.6). The momentum balances show an increase of the acceleration, and a decrease of the turbulent stress gradient. The pressure gradient remains the same, because we cannot compare it with field measurements. In the modified streamwise and transverse momentum balance, the acceleration remains larger than the turbulent stress gradient along the whole bend, while it has about the same value as the acceleration in the previous results (figure 4.8).

TABLE 5.3 - MAGNITUDES OF DIFFERENCES BETWEEN FIELD MEASUREMENTS AND MODEL OUTPUT, USED TO CALCULATE THE MODIFICATION FACTOR

	C2		C3		C4		C5		Factor
	Field	Model	Field	Model	Field	Model	Field	Model	
u	0.59	0.60	0.28	0.32	0.29	0.31	0.36	0.41	1.0
v	0.13	0.14	0.07	0.06	0.10	0.08	0.13	0.21	1.0
w	0.02	0.03	0.03	0.02	0.03	0.02	0.01	0.01	1.5
$\rho \overline{u'v'}$	0.75	4.17	2.55	6.80	1.68	5.81	0.64	1.41	0.5
$\rho \overline{u'w'}$	0.39	1.28	1.15	2.82	1.04	0.81	0.46	0.32	0.8
$\rho \overline{v'w'}$	1.13	1.22	2.74	3.65	1.49	1.92	0.58	0.39	0.8
$\rho \overline{w'w'}$	2.70	2.31	6.90	13.5	6.28	8.87	2.87	2.03	0.7

← 0.5	0.5 ← 0.67	0.67 ← 0.8	0.8 ← 1	1 → 1.25	1.25 → 1.5	1.5 → 2	2 →
-------	------------	------------	---------	----------	------------	---------	-----

Therefore, it may be interesting for further studies to pay attention to the inviscid flow assumption for these balances around the scour hole. We proposed to reject this assumption, based on our previous results, but if we take the differences between the field measurements and the model output into account, the assumption may remain assumable. However, our modification includes large simplification, so we can only use it to discuss the real behavior of the terms around the scour hole, and not to support or reject our obtained results.

The vertical momentum balance (figure 5.6c) shows after the modification a smaller dominance of the turbulent stress gradient, and an increase of the acceleration term. However, the turbulent stress gradient remains more than 2 times larger around the deepest part of the scour hole. So, this modification gives no reason to question our rejection of the inviscid flow assumption in the vertical momentum balance. However, the reduced difference from a factor 6 to a factor 2 between the turbulent stress gradient and the acceleration, shows that improving the similarity between the field measurements and the model output is an important topic for further study.

5.3 Physical interpretation

We studied the hydrodynamic processes around a scour hole in a sharp bend. The most remarkable results were found in the vertical momentum balance, which revealed a dominance of the non-hydrostatic pressure gradient and the normal stress gradient. Therefore, we will discuss the physical meaning of those two terms and try to explain how they may relate to scour hole formation and stability.

5.3.1 Non-hydrostatic pressure

The pressure along the bend is calculated from the gravity acceleration, water density, piezometric head and water depth. The only variable in this equation is the piezometric head, the others are constants. So, a deviation from hydrostatic pressure is directly related to a change of the piezometric head. The piezometric head can physically be interpreted as the water level to which the pressure may cause the water column to rise (Vermeulen, et al., 2015). Around the scour hole, the piezometric head is mostly smaller than the hydrostatic head (figure 5.7a). As shown in the results, this deviation from the hydrostatic head is mainly balanced by the vertical component of the normal stress.

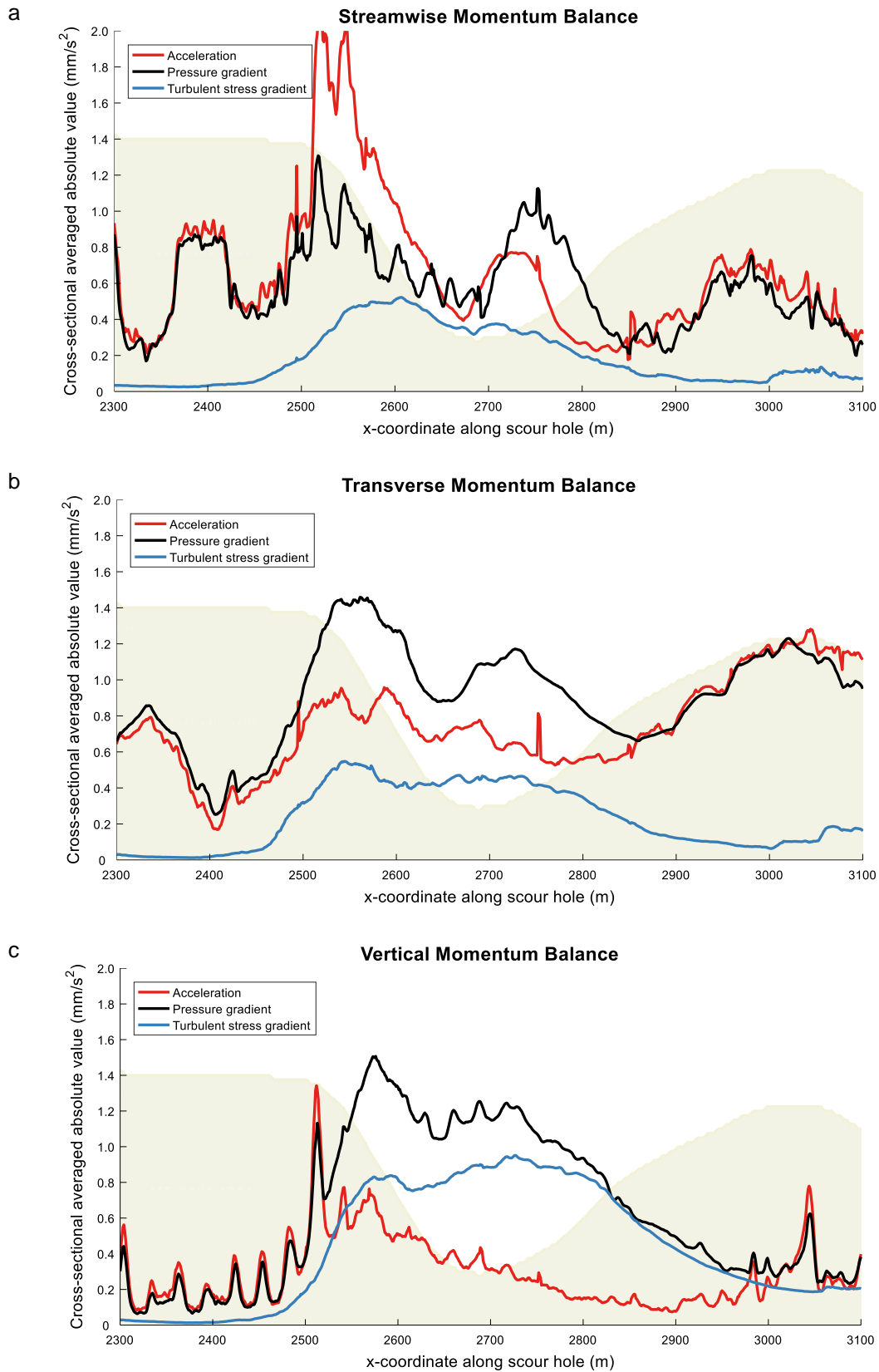


FIGURE 5.6 - MODIFIED STREAMWISE (A), TRANSVERSE (B) AND VERTICAL (C) MOMENTUM BALANCE

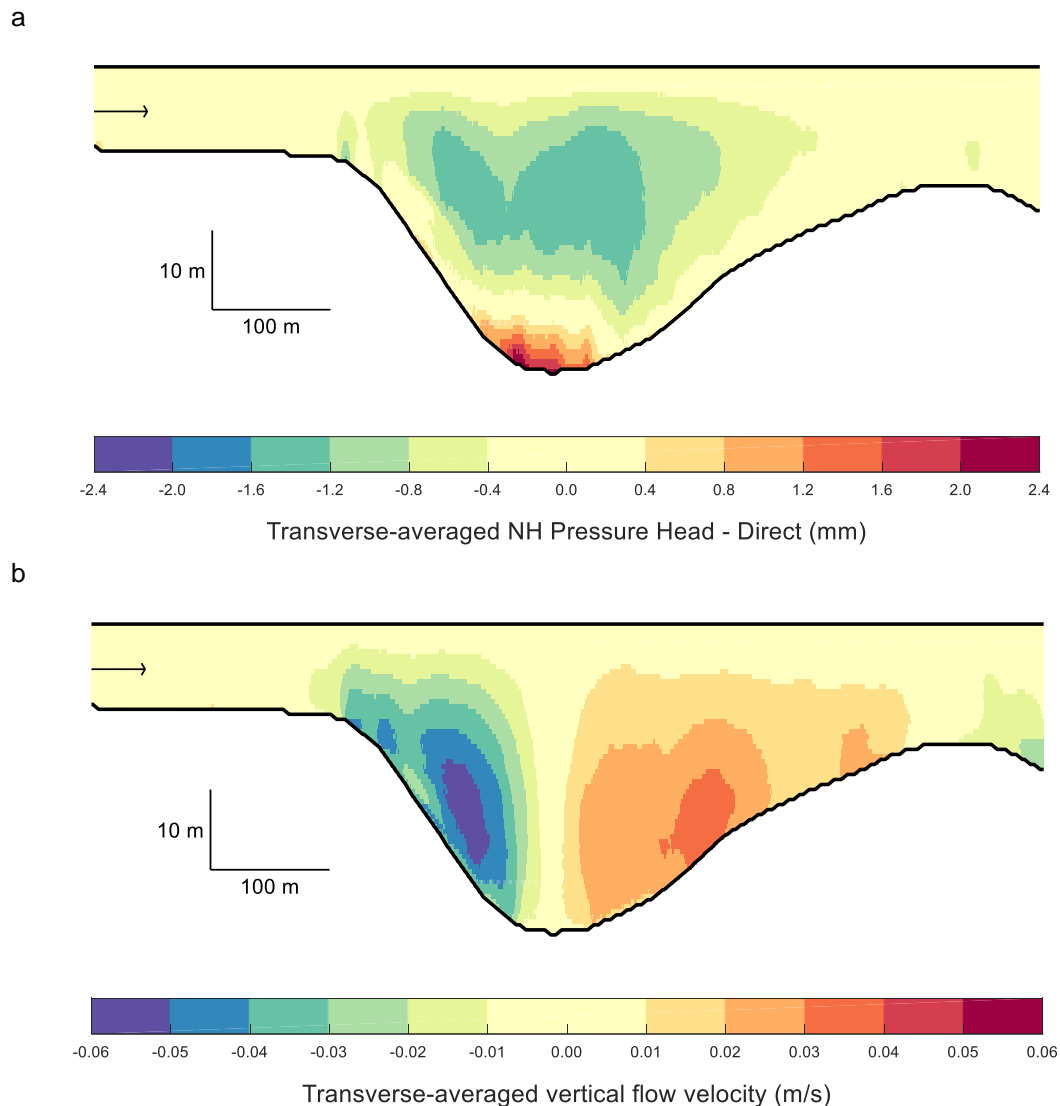


FIGURE 5.7 - TRANSVERSE-AVERAGED VERTICAL FLOW VELOCITY (A) AND NON-HYDROSTATIC PRESSURE HEAD (B) ALONG THE SCOUR HOLE

In previous studies, Vermeulen (2015) and Niesten (2016) suggested not only that the non-hydrostatic pressure is generated from vertical velocities, but also that the non-hydrostatic pressure may provide a force which curves the flow downward. We have shown that the first suggestion is not true, but the non-hydrostatic pressure may still be a driving mechanism for vertical velocity. The underlying theory is that a negative deviation from the hydrostatic head, causes the flow to curve downward at the entrance of the scour hole. We observe both in this region (figure 5.7a-b).

However, the deviation is negative along the whole scour hole (figure 5.7a), while the vertical velocity becomes positive after the deepest point of the scour hole is reached (figure 5.7b). This is in contradiction with the suggested relation. Therefore, we may conclude that we cannot explain the curvature of the streamlines throughout the scour hole only from the non-hydrostatic pressure head. Moreover, an evaluation of these streamlines shows that the curvature is rather small and may be an effect of the decelerating flow around the scour hole (figure 5.8). This supports the idea that the non-hydrostatic pressure is a direct result of the vertical component of the normal stress and that the other terms are not significantly related to this pressure.

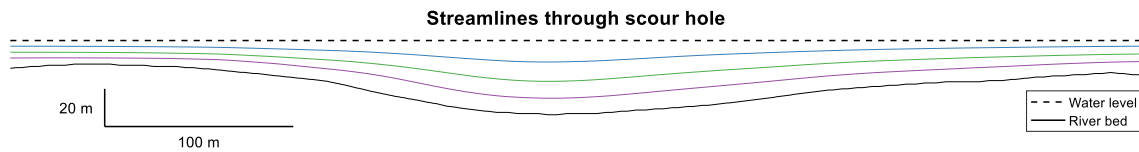


FIGURE 5.8 - STREAMLINES THROUGH SCOUR HOLE WITH EQUALLY SCALED AXES

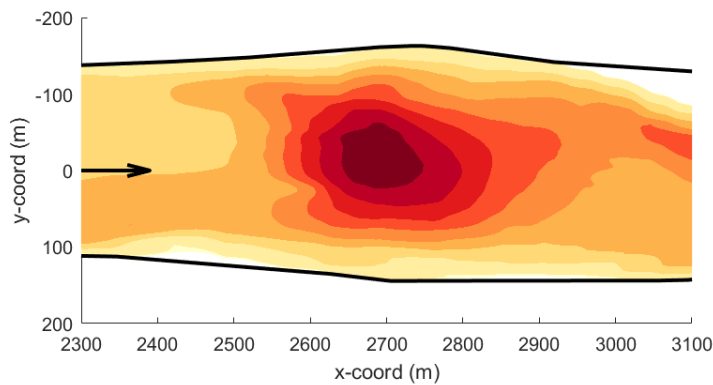


FIGURE 5.9 - COORDINATES OF TRANSFORMED MODEL OUTPUT

5.3.2 Turbulent stresses

As the deviation from the hydrostatic pressure around the scour hole is mainly generated by a large vertical component of the normal stress, it is important to understand why this turbulence shows such a huge increase. Therefore, we evaluate and compare the velocity variances in the three directions along the scour hole, because they are used to obtain the normal stresses. Thereafter, we hypothesize about the influence of large turbulent stresses towards scour hole formation and morphological stability.

Velocity variance

The results revealed a large vertical velocity variance along the scour hole and we suggested that the resulting increase of the normal stress (figure 5.10c) is caused by a larger distance from the fixed boundaries compared to the upstream channel. If such relation with the channel geometry exists, the normal stress should also increase in transverse direction, because both width and depth of the channel increase around the scour hole. The transverse normal stress shows indeed an increase in the scour hole (figure 5.10b), and also the streamwise normal stress increases (figure 5.10a).

In order to determine how the channel geometry relates to the normal stresses, we calculate their relative changes in the scour hole compared to the upstream channel. In these calculations, the values from the upstream channel are determined between x -coordinates 2300 and 2500 (figure 5.9). The differences between the upstream and peak normal stresses (table 5.4) reveal that the largest increase is found in the vertical normal stress, although its peak value is much smaller than the peak in streamwise and transverse direction.

The channel geometry shows also the largest change in vertical direction, with an increase of the depth by a factor 2.5 compared to the upstream depth, and an increase of the width by a factor 1.1. However, if we compare the changes in channel geometry with the changes in velocity variance, the changes in the velocity variances are much larger. Therefore, we suggest that the velocity variance is extremely sensitive for changes in the channel geometry. Such sensitivity was also observed by Hunt (1997), Clunie (2012), Guan et al. (2014) and Fazlollahi et al. (2015), who indicated a peak of the velocity variance around the deepest part of a pool or scour hole.

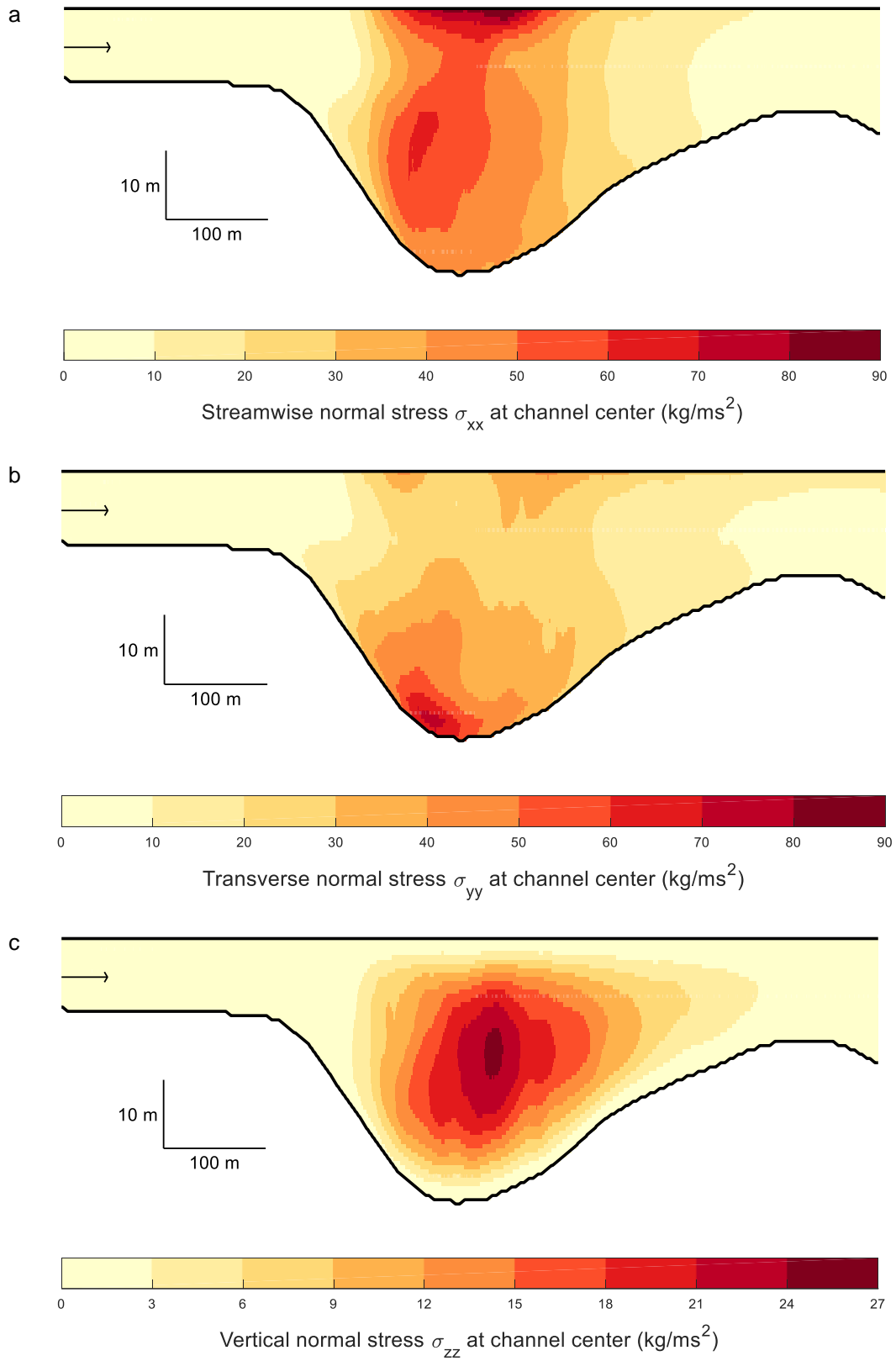


FIGURE 5.10 - STREAMWISE (A), TRANSVERSE (B) AND VERTICAL (C) NORMAL STRESSES ALONG THE SCOUR HOLE

TABLE 5.4 - CHANGE OF THE NORMAL STRESS IN THE SCOUR HOLE (KG/MS²)

	σ_{xx}	σ_{yy}	σ_{zz}
Upstream	1.96	1.44	0.04
Peak value	98	73	25
Factor	50	51	625

The similarity between the patterns of change in channel geometry and velocity variance may also reveal why the normal stress is only dominant in the vertical momentum balance. The smaller increase of the transverse velocity variance due to the smaller increase in channel width, causes a smaller gradient of the variance in transverse direction. This gradient is not large enough to make the normal stress gradient dominant in the transverse momentum balance. For the streamwise direction, we cannot relate the change in variance to a change in channel geometry, but we can see that the change of this variance in streamwise direction is small compared to the change in vertical velocity variance.

Moreover, we explained in the results that the vertical velocity variance is zero at the water surface level and the bed level. Therefore, an increase in variance will immediately increase the gradient over depth, because the difference between no variance at the channel boundaries and the peak is larger. The no flow restriction at the boundaries is not found in the streamwise and transverse velocity. So, an increase of the variance in these directions may have smaller impact on the magnitude of the gradients, because it is possible that the increase is more equally spread.

A combination of the relative large increase of the channel depth, and the restriction of no vertical flow at the channel borders causes the normal stress gradient in the vertical momentum balance to be dominant. Although the magnitudes of the normal stress in streamwise and transverse direction are much larger than in vertical direction (figure 5.10), these two reasons limit the magnitude of the gradient and so their contribution to the streamwise and transverse momentum balance.

Scour hole geometry

In our study about the dominant hydrodynamic processes in scour holes of sharp bends, we revealed large values of the non-hydrostatic pressure gradient and the normal stress gradient. We explained in the introduction that there is no agreement yet about the cause of scour hole formation and that both flow accelerations and turbulent stresses may contribute to the development of this phenomenon. From our results, we may conclude that the contribution from the flow accelerations is limited and that the turbulent stresses are the main factor in the formation of scour holes. This conclusion agrees with findings by MacVicar and Rennie (2012), who also suggested this dominance, although they admit that there is no agreement yet about the cause of scour hole formation.

Scour hole formation is caused by large sediment transport in a local area. If the bed shear stress is large enough, sediment particles move away and are not replaced. The bed shear stress can be calculated from several equations (Guan, et al., 2014). One of that equations is related to the turbulent kinetic energy (TKE). The TKE is an indicator of the total turbulent energy, and can be determined from the three components of the normal stress.

$$TKE = \frac{1}{2}(\sigma_{xx} + \sigma_{yy} + \sigma_{zz})$$

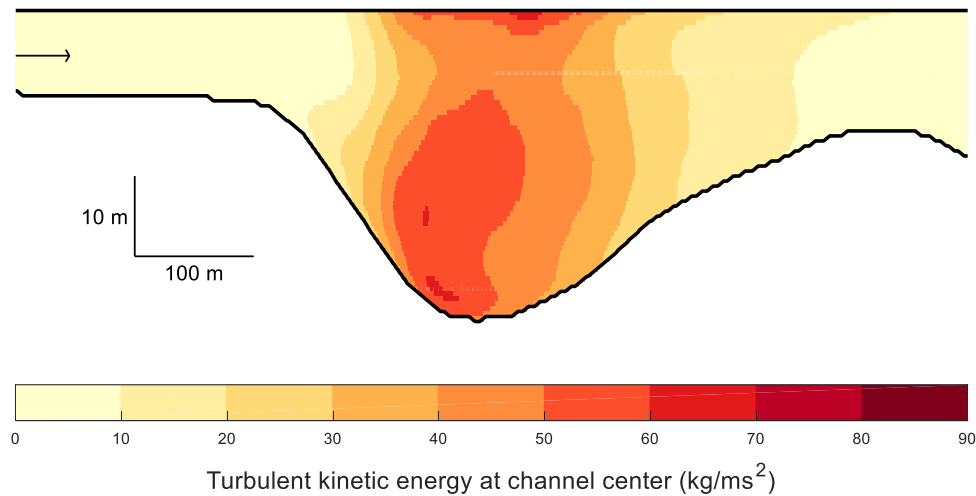


FIGURE 5.11 - TURBULENT KINETIC ENERGY ALONG THE CHANNEL CENTER OF THE SCOUR HOLE

The TKE around the scour hole shows a large increase at the entrance of the scour hole, with a peak around mid-depth, just before the deepest part of the scour hole is reached (figure 5.11). In the downstream part of the scour hole, the TKE decreases until the scour hole is passed. The large TKE may be the cause of the morphological stability of scour holes, because it makes the bed shear large enough to prevent deposition of sediments. Clunie (2012) and Guan et al. (2014) support this idea, as they also found a large TKE in a scour hole with a peak in the upstream part. However, this only explains scour hole stability and does not reveal what processes initiate scour hole formation.

Vermeulen (2014) located many deep scour holes just upstream of the highest point of curvature in sharp bends of the Mahakam River. In sharp bends, the channel geometry becomes asymmetric, with a pool in the outer bend (figure 1.1). This pool has usually a larger depth than the channel upstream of the bend. As shown in our results, an increase of the water depth has a large influence on the normal stresses. So, in the region where the depth increases upstream of the meander pool, the increase of the turbulent stresses may support the scouring and cause a deep scour hole just upstream of the highest point of curvature. However, these ideas about scour hole formation are only speculations. Much more research about the relation between the location of maximum turbulent stresses and the bend-specific processes must be done to present a reliable hypothesis about the origin of scour holes in sharp bends.

6 CONCLUSIONS

We presented a detailed study of three hydrodynamic processes in a scour hole of a sharp bend in the Mahakam River in Indonesia. We used two datasets for this analysis: field measurements and the output of a hydrodynamic model. The model somewhat under-estimates the plunging pattern of the flow into the scour hole, and overestimates the turbulent stresses. The model was previously calibrated for the three flow velocity components and shows good agreement with the field measurements (Vermeulen, et al., 2015). However, in the calibration, the turbulent stresses were not taken into account.

In our study, we revealed that these turbulent stresses are important to understand the hydrodynamic processes in scour holes of sharp bends. First, we showed that the non-hydrostatic pressure head cannot be obtained only from flow velocities, as suggested by Vermeulen et al. (2015) and Niesten (2016). We must include the vertical normal stress in the equation to find large similarity with the modelled non-hydrostatic pressure head. Next, we showed that the turbulent stress gradient in all three momentum balances becomes significant in the scour hole. Therefore, we conclude that we cannot describe the hydrodynamic processes in the scour hole with the assumption of inviscid flow.

Moreover, a detailed evaluation of the vertical momentum balance revealed the dominance of the normal stress gradient and the non-hydrostatic pressure gradient in the scour hole. They are more than 6 times larger than the other terms. A vertical normal stress originates from the variance in vertical flow velocity, which shows a huge increase in the scour hole. It seems therefore, that velocity variances are extremely sensitive to changes in the channel geometry. In further study about the origin and stability of scour holes in sharp bends, this large increase of the turbulent stresses in scour holes may be the key to understand the scouring processes.

However, we also revealed that the hydrodynamic model overestimates the velocity variances, and so the turbulent stresses. Therefore, we recommend to study possible methods to make a reliable approximation of the velocity variances from field measurements and use these values to calibrate the hydrodynamic model again. If the hydrodynamic model gives better values of the turbulent stresses, our findings will probably somewhat change, but they will also be more useful in increasing our understanding of the processes related to scour holes in sharp bends.

REFERENCES

- Alford, J. J., Baumann, R. H. & Lewis, A., 1982. Circular meander pools. *Earth Surface Processes and Landforms*, 7(2), pp. 183-188.
- Belatos, S., Carter, T. & Prowse, T., 2011. Morphology and genesis of deep scour holes in the Mackenzie Delta. *Canadian Journal of Civil Engineering*, Volume 38, pp. 638-649, doi: 10.1139/L11-034.
- Beltaos, S. et al., 2012. Flow Structure and Channel Stability at the Site of a Deep Scour Hole, Mackenzie Delta, Canada. *ARCTIC*, Issue 65, pp. 182-194.
- Blanckaert, K., 2011. Hydrodynamic processes in sharp meander bends and their morphological implications. *Journal of Geophysical Research* (116), pp. F01003, doi: 10.1029/2010JF001806 .
- Blanckaert, K., Constantinescu, G., Uijttewaal, W. & Chen, Q., 2013. Hydro- and morphodynamics in curved river reaches - recent results and directions for future research. *Advances in Geosciences*, Issue 37, pp. 19-25, doi: 10.5194/adgeo-37-19-2013.
- Blanckaert, K. & Graf, W. H., 2001. Experiments on flow in an open-channel bend. Mean flow and turbulence. *Journal of Hydraulic Engineering*, 127(10), pp. 835-847.
- Blanckaert, K. & Vriend, H. J. d., 2004. Secondary flow in sharp open-channel bends. *Journal of Fluid Mechanics*, Issue 498, pp. 353-380; doi: 10.1017/S0022112003006979.
- Blanckaert, K. & Vriend, H. J. d., 2010. Meander dynamics: A nonlinear model without curvature restrictions for flow in open-channel bends. *Journal of Geophysical Research*, Volume 115, pp. F04011, doi: 10.1029/2009JF001301.
- Booker, D. J., Sear, D. A. & Payne, A. J., 2001. Modelling three-dimensional flow structures and patterns of boundary shear stress in a natural pool-riffle sequence. *Earth Surface Processes and Landforms*, Volume 26, pp. 553-576, doi: 10.1002/esp.210.
- Clunie, T. M., 2012. *Flow Over Fluvial Bedforms*, Auckland: The University of Auckland.
- Corney, R. K. T. et al., 2006. The orientation of helical flow in curved channels. *Sedimentology* , Volume 53, pp. 249-257, doi: 10.1111/j.1365-3091.2006.00771.x.
- Crosato, A., 2008. *Analysis and modelling of river meandering*. 1 ed. Amsterdam: IOS Press.
- Fassnacht, S. R. & Conly, F. M., 2000. Persistence of a scour hole on the East Channel of the Mackenzie Delta. *Canadian Journal of Civil Engineering*, 27(4), pp. 798-804.

- Fazlollahi, A., Afzalimehr, H. & Sui, J., 2015. Effect of slope angle on an artificial pool on distributions of turbulence. *International Journal of Sediment Research*, Volume 30, pp. 93-99, doi: 10.1016/j.ijsrc.2015.03.008.
- Fox, R. W., McDonald, A. T. & Pritchard, P. J., 2011. *Fluid Mechanics*. Asia: Wiley.
- Gharabaghi, B., Inkratas, C., Beltaos, S. & Krishnappan, B., 2007. Modelling of three-dimensional flow velocities in a deep hole in the East Channel of the Mackenzie Delta, Northwest Territories. *Canadian Journal of Civil Engineering*, 34(10), pp. 1312-1323.
- Guan, D., ASCE, B. W. M. M. & Friedrich, H., 2014. Flow Patterns and Turbulence Structures in a Scour Hole Downstream of a Submerged Weir. *Journal of Hydraulic Engineering*, 140(1), pp. 68-76, doi: 10.1061/(ASCE)HY.1943-7900.0000803.
- Huismans, Y., Van, G., O'Mahoney, T. & Wiersma, A., 2016. *Scour hole development in river beds with mixed sand-clay-peat stratigraphy*. Oxford, CRC Press.
- Hunt, A. E., 1997. *The behaviour of turbulence in unsteady open channel flow*, Canterbury: University of Canterbury.
- Kim, D. & Muste, M., 2012. Multi-dimensional representation of river hydrodynamics using ADCP data processing software. *Environmental Modelling & Software*, Volume 38, pp. 158-166, doi: 10.1016/j.envsoft.2012.05.011.
- Klingeman, P. C., Kehe, S. M. & Owusu, Y. A., 1984. *Streambank Erosion Protection and Channel Scour Manipulation Using Rockfill Dikes and Gabions*. 1 ed. Corvallis: United States Department of the Interior.
- Koh, 2011. *The geographical empanadas*. <https://sites.google.com/site/thegeographical-empnadas2011/revision-helper-for-rivers>.
- MacVicar, B. J. & Rennie, C. D., 2012. Flow and turbulence redistribution in a straight artificial pool. *Water resources research*, Volume 48, pp. W02503, doi: 10.1029/2010WR009374.
- MacWilliams, M. L. et al., 2006. Flow convergence routing hypothesis for pool-riffle maintenance in alluvial rivers. *Water Resources Research*, Volume 42, pp. W10427, doi: 10.1029/2005WR004391.
- Nanson, R. A., 2010. Flow fields in tightly curving meander bends of low width-depth ratio. *Earth Surface Processes and Landforms*, Volume 35, pp. 119-135, doi: 10.1002/esp.1878.
- Nielsen, I., 2016. *Deviations from the hydrostatic pressure distribution retrieved from ADCP velocity data*, Wageningen: Wageningen University.
- Nieuwstadt, F. T. M., 1998. Directe en "large eddy"-simulatie van turbulentie. In: *Turbulentie*. Utrecht: Epsilon Uitgaven, pp. 142-148.
- Nystrom, E. A., Rehmann, C. R., ASCE, M. & Oberg, K. A., 2007. Evaluation of Mean Velocity and Turbulence Measurements with ADCPs. *Journal of Hydraulic Engineering*, 133(12), pp. 1310-1318, doi: 10.1061/(ASCE)0733-9429(2007)133:12(1310).
- Ottevanger, W., 2013. *Modelling and parameterizing the hydro- and morphodynamics of curved open channels*. Delft: Ipskamp Drukkers; ISBN: 978-94-6191-925-0.
- Ottevanger, W., Blanckaert, K. & Uijttewaal, W., 2012. Processes governing the flow redistribution in sharp river bends. *Geomorphology*, 163(164), pp. 45-55, doi: 10.1016/j.geomorph.2011.04.049.
- Rhoads, B. L. & Kenworthy, S. T., 1995. Flow structure at an asymmetrical stream confluence. *Geomorphology*, Volume 11, pp. 273-293.
- Sawatsky, L. F., Bender, M. J. & Long, D., 1998. *Pipeline exposure at river crossings: causes and cures*. Canada, ASME.

Schnauder, I. & Sukhodolov, A. N., 2012. Flow in a tightly curving meander bend: effects of seasonal changes in aquatic macrophyte cover. *Earth Surface Processes and Landforms*, Issue 37, pp. 1142-1157, doi: 10.1002/esp.3234.

Tan, S.-K., Yu, G., Lim, S.-Y. & Ong, M.-C., 2005. Flow Structure and Sediment Motion around Submerged Vanes in Open Channel. *Journal of Waterway, Port, Coastal, and Ocean Engineering*, 131(3), pp. 132-136.

Teledyne RD Instruments, 2006. *ADCP - Principles of Operation - A Practical Primer*. 2 ed. California: Teledyne RD Instruments.

Venditti, J. G. et al., 2014. Flow in bedrock canyons. *Nature*, 513 (7519), pp. 534-537; doi: 10.1002/esp.3290070603.

Vermeulen, B., 2014. *Rivers running deep*. Wageningen: ISBN: 978-94-6257-206-5.

Vermeulen, B., Hoitink, A. J. F., Berkum, S. W. v. & Hidayat, H., 2014. Sharp bends associated with deep scour holes in a tropical river: The river Mahakam (East Kalimantan, Indonesia). *Journal of Geophysical Research: Earth Surface*, Issue 119, pp. 1441-1454; doi:10.1002/2013JF002923.

Vermeulen, B., Hoitink, A. J. F. & Labeur, R. J., 2015. Flow structure caused by a local cross-sectional area increase. *Journal of Geophysical Research: Earth Surface*, Issue 120, pp. 1771-1783, doi: 10.1002/2014JF003334.

Vermeulen, B. et al., 2015. *Including generic models in repeat-transect ADCP data processing*. Erfurt, IAHR2015 World Congress.

Vermeulen, B., Sassi, M. G. & Hoitink, A. J. F., 2014. Improved flow velocity estimates from moving-boat ADCP measurements. *Water Resources Research*, Volume 50, pp. 4186-4196, doi: 10.1002/2013WR015152.

APPENDICES

A. Local balances

In the evaluation of the hydrodynamic processes we used the cross-sectional averaged absolute values. However, taking these averages may result in wrong patterns, due to both positive and negative values within a cross-section. Therefore, we evaluated the hydrodynamic processes also on a local scale (figure A.1). The evaluated local area has a width of 40 meters, and a height of 6 meters and can be found around the channel center 2.5 meters below the water surface. The momentum balances (figure A.2) show the same patterns of dominant terms as in the balances with the cross-sectional averaged values. However, the values in the local balances are a bit larger than in balances with the average terms.

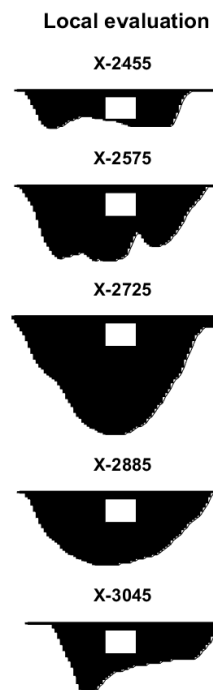


FIGURE A.1 - AREAS OF LOCAL EVALUATION OF HYDRODYNAMIC PROCESSES

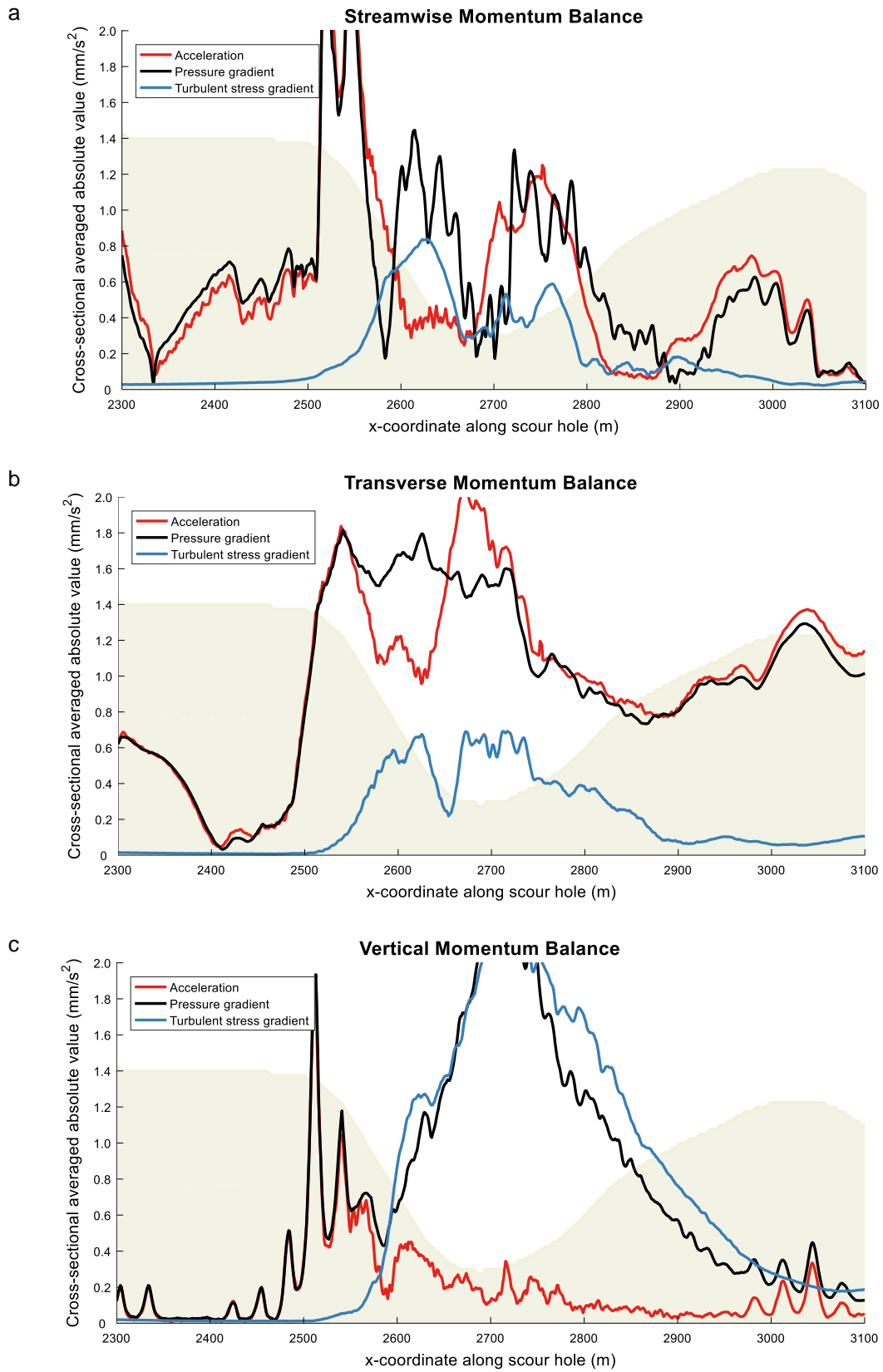


FIGURE A.2 - HYDRODYNAMIC PROCESSES IN STREAMWISE (A), TRANSVERSE (B) AND VERTICAL MOMENTUM BALANCE

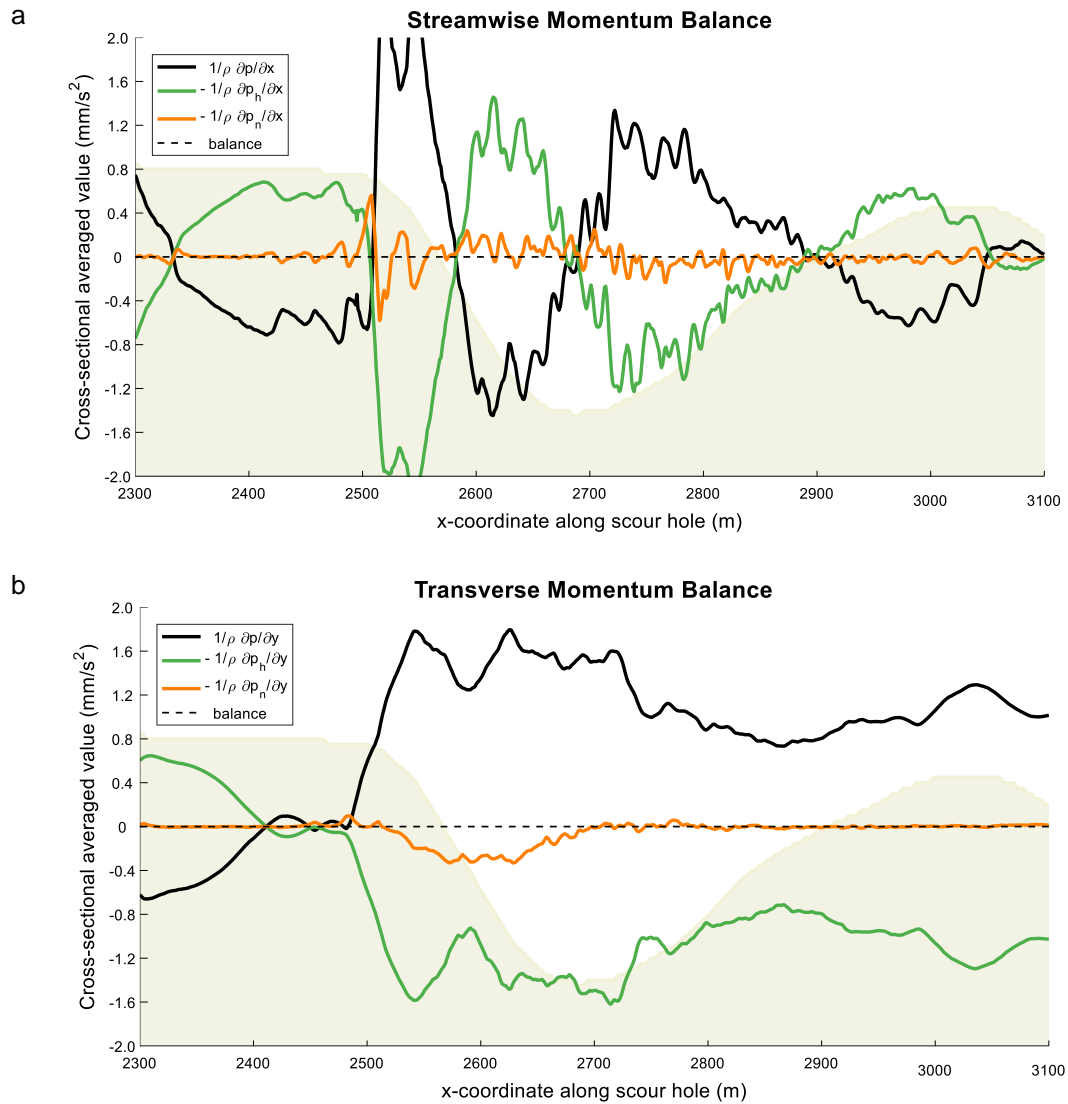


FIGURE A.3 - HYDROSTATIC AND NON-HYDROSTATIC PRESSURE GRADIENT IN STREAMWISE (A) AND TRANSVERSE (B) MOMENTUM BALANCE

We also evaluated the local balances for the pressure gradients (figure A.3). They show also the same patterns as in the cross-sectional averaged balances. The contribution of the non-hydrostatic pressure gradient in the transverse balance at the entrance of the scour hole is larger in this local area.

B. Extensive balances

We showed the streamwise and transverse momentum balances in the results only with the average acceleration and turbulent stress gradient. However, the patterns in these balances show good agreement with the balances where all terms are presented (figure A.4). The most remarkable differences are the dominance of the acceleration in streamwise direction above the other two accelerations, and the normal stress gradient in the streamwise momentum balance, which remains close to zero along the whole scour hole.

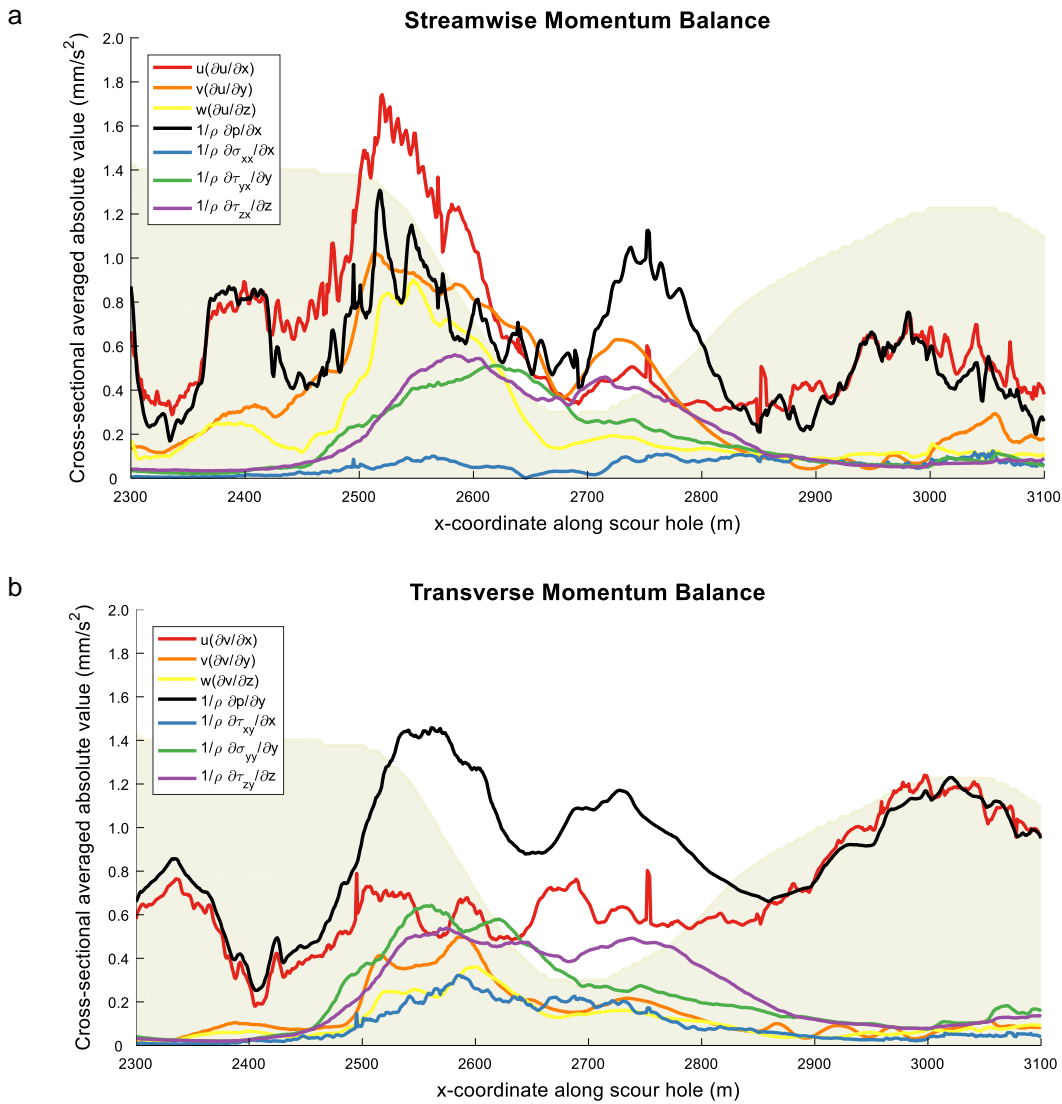


FIGURE A.4 - CROSS-SECTIONAL AVERAGED VALUES OF THE TERMS IN THE STREAMWISE (A) AND TRANSVERSE (B) MOMENTUM BALANCES